Development of ^{18}F Radiochemistry for Positron Emission Particle Tracking (PEPT)

Ameerah Camroodien

Department of Physics
University of Cape Town

Dissertation presented to the University of Cape Town in fulfilment of the
academic requirements for
Master of Science degree in Physics

October 2023

Declaration

I hereby declare that the contents of this dissertation are original and have not been submitted in whole or in part for consideration for any other degree or qualification in this, or any other university. This dissertation is my own work and contains nothing which is the outcome of work done in collaboration with others, except as specified in the text with due reference to the literature and Acknowledgements.

Ameerah Camroodien
October 2023

Acknowledgements

I would like to express my gratitude to my supervisor, Dr. Tom Leadbeater, for providing guidance and insight into the broader picture of this research. Thank you for redirecting me to the right path in this research and encouraging me to keep persisting.

Thank you to my co-supervisor, Dr. Shankari Nair, for going the extra mile to ensure all resources were available and providing reassurance during uncertain times. I appreciate your tenacity in experimental problem solving and inspiration throughout this research.

To Mike van Heerden, I am indebted to your patience. Thank you for sharing your expertise and guiding me every step of the way with kindness. I appreciate your dedication to ensuring my well-being and safety was never compromised during experimental work.

I would like to acknowledge and thank the National Research Foundation (NRF) accelerator facility iThemba LABS Nuclear Medicine Department for the supply of ^{18}F-fluorodeoxyglucose (^{18}F-FDG) throughout this research.

I would also like to thank NRF for funding this Masters of Science degree.

Last but not least, I would like to express my appreciation to my mother and sister for all their support in this journey.

Research Contributions

Presentation, July 2021
Development of ^{18}*F Radiochemistry for Positron Emission Particle Tracking (PEPT)*, presented at the **65th Annual Conference of the South African Institute of Physics (SAIP 2021)**, 22 - 30 July 2021, South Africa.

Conference Proceedings, 2022
Development of ^{18}*F Radiochemistry for Positron Emission Particle Tracking (PEPT)*, **The Proceedings of SAIP 2021**, 2022.

Poster Presentation, September 2022
Development of ^{18}*F Radiochemistry for Positron Emission Particle Tracking (PEPT)*, presented at the **28th International Nuclear Physics Conference (INPC 2022)**, 11 - 16 September 2022, South Africa.

Conference Proceedings (co-author), 2023
Dynamics of physical flows measured by positron emission techniques, **The Proceedings of INPC 2022**, 2023.

Conference Proceedings (co-author), 2023
Dynamics of physical flows measured by positron emission techniques, **The Proceedings of INTDS 2022, 30th Conference of the International Nuclear Target Development Society**, 2023.

Journal (co-author), 2023
Development of tracer particles for positron emission particle tracking (PEPT), *Nuclear Science and Engineering*, **197**, Issue 3, 2023.

Abstract

Positron emission particle tracking (PEPT) is a non-invasive tracer-based measurement technique used to obtain dynamic information about multiphase systems. The basis of the technique is to radiolabel a phase-representative tracer particle with a positron emitting radionuclide. Electron-positron annihilation produces pairs of back-to-back 511 keV gamma photons emitted from the locality of the tracer particle. Pairs of annihilation photons are detected within the field-of-view of a modified positron emission tomography (PET) scanner, and the instantaneous position of the tracer particle is determined in three dimensions using reconstruction of consecutive annihilations via an iterative algorithm. From the continuously measured tracer particle trajectory, the time differential is used to produce velocity (and acceleration) fields, and further trajectory analysis reveals the localised behaviour of the tracer in the system under study including residence times and kinematic properties. For optimum tracking the radioactivity in a single particle must be sufficient irrespective of the tracer size and material. Typically activities in the range 250 μCi – 2 mCi are required, often loaded on to particles in the 10 mm – 100 μm diameter range. The physical properties of the tracer must accurately reflect those of the bulk media under study such that the measured PEPT data is reflective of the bulk motion.

In this research a novel radiochemical technique in producing tracer particles from commercially available medical grade ^{18}F-fluorodeoxyglucose (^{18}F-FDG) (half-life 110 minutes) was developed. In the context of the radioisotopes and accelerated beams available through the National Research Foundation (NRF) accelerator facility iThemba LABS (Cape Town, South Africa), these methods offer the best, perhaps only, mechanism to utilising ^{18}F-based radiotracers for PEPT in South Africa. Furthermore, this work reduces the need for daily isotope production by a dedicated cyclotron beam and the need for specialist equipment. Provided a suitable source of medical ^{18}F-FDG can be sourced, PEPT is therefore possible without the site constraints of an accelerator facility, enabling wider applications of the technique. Compared to the ^{68}Ga-based tracer particles (half-life 68 minutes) pioneered by PEPT Cape Town, ^{18}F based tracers have the distinct advantages of a longer half-life allowing for extended experimental timescales, and an increased signal to noise ratio from

the pure β^+ emission with no additional gamma transitions.

Commercially available medical grade ^{18}F-FDG was utilised as the initial ^{18}F stock. A column chromatography method was developed to separate the glucose-complex of ^{18}F-FDG in preparation of the reactive solution, made of ^{18}F in trifluoroacetic acid (TFA) complex, and used for radiolabelling. The anion exchange resins Purolite A870 and A200 were investigated for their ability to exchange non-radioactive counter ions for the required species. Ion exchange techniques were used to label small phase-representative tracer particles (< 1 mm diameter) by controlled uptake of ^{18}F.

With limiting abundance effects, a loading solution composition of 1:2.5 of TFA:^{18}F-FDG provided greatest uptake and activities of up to 100 μCi and 80 μCi were achieved for the A870 and A200 resins of diameter ranging from 430 - 590 μm respectively. The radiolabelling method was adjusted to incorporate pre-treatment of the reactive solution prior to radiolabelling and yielded improved radiolabelling performance, resulting in 300 μCi and 200 μCi activities for the A870 and A200 resins of diameter ranging from 550 - 610 μm respectively. While the activity is still low with regards to optimum tracking, the methods developed here show potential for future tracer particle production. In some applications, particularly those with low attenuation and photon scattering, and/or small scale systems, the particles developed here are ideal.

Abbreviations

^{18}F-FDG	^{18}F-fluorodeoxyglucose
AC	Activity concentration
ADC	Analogue to digital converter
BGO	Bismuth germinate
CAD	Coronary artery disease
CH_3OH	Methanol
CoM	Centre-of-mass
DVB	Divinylbenzene
FWHM	Full width at half maximum
HCl	Hydrochloric acid
HPGe	High purity germanium
KF	Potassium fluoride
LOR	Line of response
NaI	Sodium iodide
NaI(Tl)	Thallium-activated sodium iodide
NRF	National Research Foundation
o-Ps	Ortho-positronium
PEPT	Positron emission particle tracking
PET	Positron emission tomography
PIC	Positron Imaging Centre
p-Ps	Para-positronium
SA	Specific activity
SA_{max}	Maximum specific activity
SiO_2	Silicone dioxide
SPC2	Light-ion Solid-pole Injector Cyclotron
SPECT	Single-photon emission computed tomography
SSC	Separated Sector Cyclotron
TFA	Trifluoroacetic acid
UCT	University of Cape Town

Table of contents

List of Figures

List of Tables

Chapter 1

Introduction and Background

Positron emission particle tracking (PEPT) is a non-invasive measurement technique used to obtain dynamic information about multiphase systems. The basis of the technique is to radiolabel a phase-representative tracer particle with a suitable positron emitting radionuclide, with electron-positron annihilation producing pairs of back-to-back 511 keV gamma photons. When consecutive pairs of photons are detected within the field-of-view of a modified positron emission tomography (PET) scanner, the instantaneous position of the tracer particle is determined using reconstruction of consecutive annihilations via an iterative algorithm.

In order for the measured PEPT data to be reflective of the motion under study, the radioactivity in a single particle must be sufficient irrespective of the tracer size and the physical properties of the material under study must be representative of the media under study. PEPT Cape Town has pioneered the use of ^{68}Ga (half-life 68 minutes) in tracer particle fabrication, however in this research a novel radiochemical technique producing tracer particles using the radioisotope ^{18}F (half-life 110 minutes) was developed. Advantageously ^{18}F is a pure β^+ emitter with no additional gamma emissions, therefore increasing the signal to noise ratio in PEPT measurements. Additionally the longer half-life of ^{18}F allows for extended experimental timescales in comparison to ^{68}Ga.

1.1 The nature of radioisotopes

Isotopes of an element are nuclides that have the same atomic number but different numbers of neutrons and therefore different mass numbers [1]. For example, two utilised isotopes of fluorine are ^{19}F and ^{18}F, with ^{19}F being the most abundant and only naturally occurring stable isotope of fluorine and ^{18}F being artificially produced. Unstable isotopes tend in time to change to achieve stable configurations via various processes termed as radioactive decay

[2]. These radioactive decay processes occur through the emission of a charged particle (α, β^+ or β^-), resulting in a nucleus with a different electric charge and chemically different element [2,3]. Electromagnetic radiation in the form of gamma rays or X-rays are emitted as a result of de-excitation of the daughter nucleus following disintegration.

Beta decay occurs when an unstable nucleus decays into another nucleus and emits either a positron (e^+) and a neutrino (v_e) or an electron (e^-) and an antineutrino ($\bar{v}_e$); in particular β^+-decay occurs inside a proton-rich nuclide in which a proton is converted into a neutron while releasing a positron and a neutrino [3].

^{18}F decays dominantly (97%) via β^+-decay as described by the reaction,

$$^{18}_{9}\mathrm{F} \rightarrow {}^{18}_{8}\mathrm{O} + {}^{0}_{1}e + v_e, \tag{1.1}$$

such that ^{18}F decays to ^{18}O releasing a neutrino and a positron. Each beta decay transition is characterised by a decay energy known as the reaction Q-value, where the Q-value expresses the energetics of nuclear reactions and is defined as the difference between the sum of the masses of the initial reactants and the sum of the masses of the final reaction products in energy units [2]. In the decay energy is shared among the three products and momenta proportional such that the momentum of the initial nucleus in its centre-of-mass (CoM) frame is equal to the momentum of the components after the decay. The positron energy varies in different decays from zero to the endpoint energy, which is equivalent to the Q-value. The positron is typically produced with an energy equivalent to a significant fraction of the Q-value, thus resulting in maximum velocity, and the positron will pass through materials and lose kinetic energy through excitation and ionisation of the surrounding material electrons through long range Coulomb elastic and in-elastic scattering [4]. The positron loses energy partially by Cerenkov emission [5] until it reaches thermal equilibrium with the surrounding electrons. When the positron and electron have the same momenta in the lab frame and/or the CoM momenta is zero, the positron and electron may form a bound state, a positronium, or may annihilate directly.

Positronium is a short-lived bound state hydrogen-like atom of a positron and an electron with zero net charge and decays by the electromagnetic interaction into two or more gamma rays [6]. In following conservation laws, annihilation of the electron-positron pair and resultant two gamma rays ensures that net charge as well as linear momentum are conserved [7]. Additionally the total energy of the positronium before annihilation must be shared between the produced gamma rays.

Positronium is distinguished according to their relative spin orientation, namely the singlet state as para-positronium (p-Ps) with average lifetime of 0.124 ns and the triplet state ortho-positronium (o-Ps) with average lifetime 138 ns [6]. To conserve spin angular momentum, the singlet and triplet state can only decay into an even and odd number of gamma rays respectively. However, the leading decay for the single state is two gamma rays and for the triplet state it is three gamma rays as the branching ratio decreases as the number of resultant gamma rays increases [6,8]. Assuming it is equally likely that a captured positron has spin parallel or antiparallel to that of the capturing electron, and the spin conversion rate from o-Ps to p-Ps is about 4 times that of p-Ps to o-Ps [8], the difference in the average lifetimes between the two states indicates that p-Ps will outweigh o-Ps available for decay per emission event [7], therefore two gamma ray annihilations are highly probable.

Recall that the relativistic energy of a photon is given by [4]

$$E = \sqrt{m_\gamma^2 c^4 + p^2 c^2} = pc, \tag{1.2}$$

where a photon has no rest mass. With the p-Ps at rest, this equipartition of energy can be expressed as [7]

$$\sqrt{4m_e^2 c^4 + p_{p-Ps}^2 c^2} = 2m_e c^2 = p_1 c + p_2 c = 2pc = 2E_\gamma, \tag{1.3}$$

where it indicates both gamma rays have rest mass energy of 511 keV.

In abridgement, the annihilation probability is maximal when the positron and electron are in thermal equilibrium. The annihilation usually releases a minimum of two photons with the two photon emission being exactly equal and opposite in momenta in the CoM frame of the electron-positron pair. Therefore, if the positron annihilates with energy above thermal, then the two photon emission is not constrained to be back-to-back (the angle then depends on the energy) and will not assist in positron imaging.

Electromagnetic radiation results from the positron-electron annihilation where two photons, each with energy 511 keV, are emitted nearly back-to-back as depicted in Fig. 1.1. Different radionuclides exhibit various decay schemes and consequently varying radiations emitted and corresponding energies. ^{18}F has a mass of 18 amu and its half-life is 110 minutes [10]. It decays by positron emission 97% of the time and electron capture 3% of the time, however both yield stable ^{18}O.

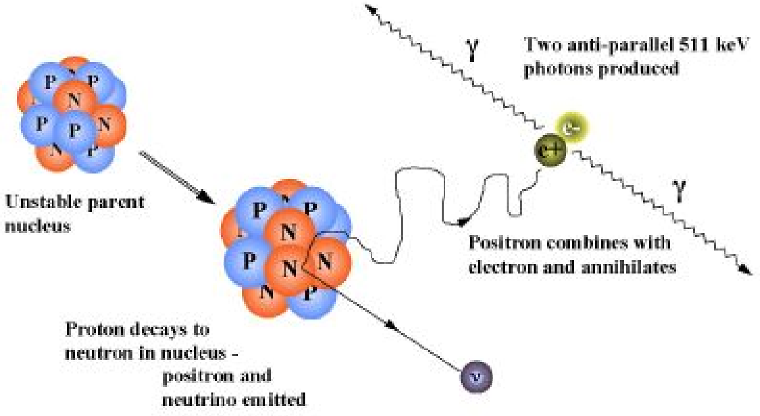

Fig. 1.1 Illustration of the positron emitted via β^+-decay. The positron encounters electrons in surrounding matter and collide, such that positron-electron annihilation results in the emission of two nearly colinear 511 keV photons [9].

All radioactive materials decay according to the following equation,

$$\frac{dN}{dt} = -\lambda N, \tag{1.4}$$

where dN/dt is the disintegration rate in seconds and λ is the decay constant in reciprocal seconds ($\lambda = \ln(2)/t_{1/2}$) [2,10]. The time for the activity to fall to half its initial value, the half-life, is

$$t_{1/2} = -\frac{\log_e 0.5}{\lambda} = \frac{0.693}{\lambda}. \tag{1.5}$$

Specific activity (SA) is a measure of the number of radioactive atoms or molecules as compared with the total number of those atoms or molecules present in the sample and typically expressed in radiation units per mass unit [2]. Using the above equations, the proportion of a radionuclide remaining after a set time can be determined as well as the maximum specific activity, SA_{max}, which is theoretically a measure if all molecules are labelled with a radioisotope. For example, one gramme of a radioisotope will contain

$$\frac{6.02 \times 10^{23}}{W} \quad \text{atoms}, \tag{1.6}$$

where W is the atomic mass of the radioisotope. A fraction λ will disintegrate each second and with 1 Curie (Ci) = 3.7×10^{10} disintegrations per second, the activity of one gramme of pure radioisotope is [10]

$$\mathrm{SA_{max}} = \frac{6\times10^{23}}{3.7\times10^{10}}\cdot\frac{\lambda}{\mathrm{W}} = \frac{6\times10^{23}}{3.7\times10^{10}}\cdot\frac{0.693}{\mathrm{W.t_{1/2}}}, \tag{1.7}$$

where $t_{1/2}$ is in seconds. Substituting $\mathrm{W}_{^{18}\mathrm{F}}$ = 18 amu and $t_{1/2}(^{18}\mathrm{F})$ = 6600 s, the atomic weight of ^{18}F and half-life of ^{18}F in seconds respectively, the activity of 1 g of pure ^{18}F is 9.45×10^7 Ci/g.

In relation, radioactive substances can also be expressed by the activity concentration (AC) which is defined as the ratio of the activity of a radionuclide to the volume of the material in which the radionuclide is uniformly distributed.

In addition to the electromagnetic radiations emitted, the fact that isotopes of an element have nearly identical chemical behavior as stable isotopes of the same element [11] motivates the applications of radioisotopes across scientific and medical disciplines, with particular understanding of the energies and radiations emitted needed prior to selection of a radioisotope. Isotopes of an element have identical chemical properties, such as acidity, flammability and chemical stability. Physical properties such as mass, melting or boiling point and density will depend on the mass of each isotope. It is therefore impactful to examine how radioisotopes are produced before they can be implemented further.

1.1.1 Radioisotope production

Radionuclide production involves altering the number of protons and/or neutrons of a target nuclide in order to produce the resulting nuclide. This is typically achieved by bombardment using a nuclear reactor or accelerator where neutron bombardment generally yields neutron-rich isotopes and decay via β^--decay, whereas charged particle bombardment generally yields neutron-deficient isotopes and decay via β^+-decay or electron capture [10]. In order to produce a specific radionuclide the corresponding target nucleus and the appropriate nuclear reaction, with careful selection of the bombarding particle and its energy, is required.

Nuclear activation reactions are denoted in the form of $^{\mathrm{Z+N}}\mathrm{A(x,y)}^{\mathrm{Z'+N'}}\mathrm{B}$ where x and y represent the incident particle and the particle or photon emitted respectively. A denotes the initial nuclide with corresponding proton and neutron numbers of Z and N respectively, and B denotes the product nuclide with corresponding proton and neutron numbers of Z' and N' respectively.

Considering a beam of particles bombarding a target or material, there is some probability that some reaction will take place. For this the microscopic cross section σ, is essentially the effective area of the nucleus for that particular reaction. In other words that area perpendicular to the direction of the radiation is alloted to the nucleus to account geometrically for its interaction with the radiation [10].

The Table of Nuclides, with an arbitrary target shown in Fig. 1.2, is a two-dimensional representation of isotopes of elements. Here the horizontal axis represents the number of neutrons and the vertical axis represents the atomic number. This displays nuclides according to their number of protons and neutrons with relevant nuclear characteristics such as half-life, decay profiles, energies and more.

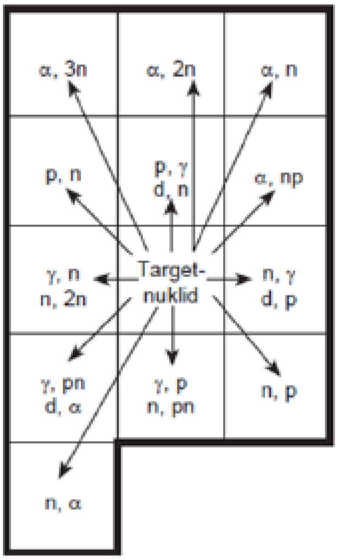

Fig. 1.2 Depiction of nuclear reaction channels for an arbitrary target [12].

Fig. 1.2 only displays the nuclear reactions with large microscopic cross sections, however ^{18}F can be produced via any of the following reactions:

- ^{18}O(p,n)^{18}F, or
- ^{20}Ne(d,α)^{18}F, or
- ^{16}O(^{3}He,p)^{18}F, or
- ^{16}O(^{3}H,n)^{18}F.

Out of all ^{18}F production methods, the reactions ^{18}O(p,n)^{18}F and ^{20}Ne(d,α)^{18}F are the two common reactions utilised [13].

The rate of radionuclide production is dependent on several factors such as the reaction cross-section as a function of energy, the incident particle energy, the thickness of the target and the flux of incoming particles which is related to the beam current. The rate of production is given by [2]

$$-\frac{dn}{dt} = R = nI\left(\left(1-e^{-\lambda t}\right)\int_{E_s}^{E_0} \frac{\sigma(E)}{dE/dx}dE, \tag{1.8}$$

where R is the number of nuclei formed per second, n is the target thickness in nuclei per cm^2, I is the incident particle flux per second and is related to the beam current, λ is the decay constant, t is the irradiation time in seconds; σ is the reaction cross-section in cm^2, E is the energy of the incident particles, x is the distance travelled by the particle and $\int_{E_s}^{E_0}$ is the integral from the initial to final energy of the incident particle along its path.

Experimentally this can be simplified for an arbitrary process i where the beam current is constant over the bombardment, if the target nuclei are uniformly distributed in the target material and the cross section is independent of energy over the incident energy range used [2]:

$$R_i = Inx\sigma_i. \tag{1.9}$$

For short lived nuclides, the rate of production and decay of the resultant nuclide will equilibrate over a particular duration of the irradiation, which is known as saturation, such that the amount of radioactivity remains constant [2,10]. The rate of formation here can be expressed as

$$R = \frac{N\lambda}{1-e^{-\lambda t}}, \tag{1.10}$$

where R is the rate of formation of nuclei, N is the number of target nuclei present at the end of the process, λ is the decay constant and the saturation factor is defined as $1-e^{-\lambda t}$ where t is the irradiation time. In actuality the production limits of a given radionuclide are determined by the half-life and the length of irradiation needs to be considered in conjunction with the desired yield. Specific activity reaches a saturation for large t values and does not build up indefinitely. Activity typically reaches half of the final saturation in an irradiation time in duration to one half-life [10].

As mentioned, the reactions ^{18}O(p,n)^{18}F and ^{20}Ne(d,α)^{18}F are the two common reactions utilised for producing ^{18}F. From Fig. 1.3 and Fig. 1.4 the maximum yield occurs at less than 10 MeV and they both have thresholds of 0 - 2 MeV, however the ^{18}O(p,n)^{18}F pathway has a higher cross section.

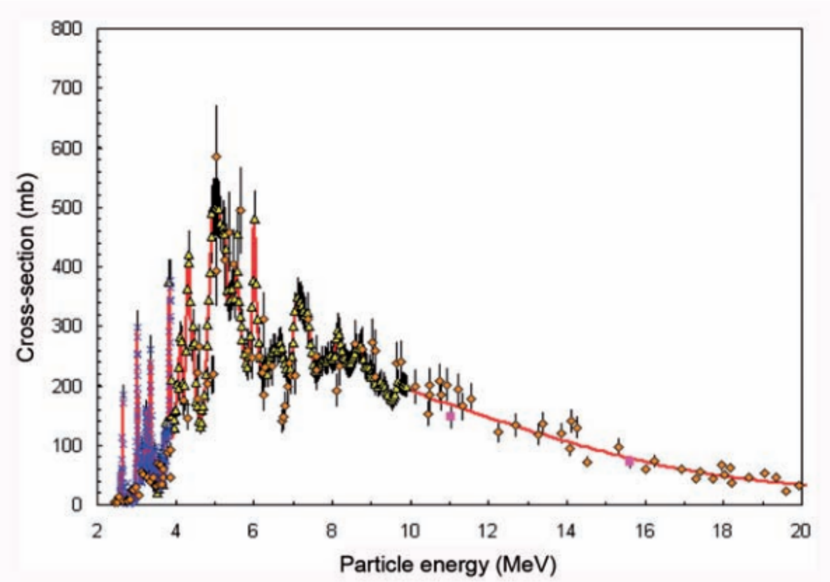

Fig. 1.3 Yield for the ^{18}O(p,n)^{18}F reaction pathway as a function of the energy dependence of the cross section [2].

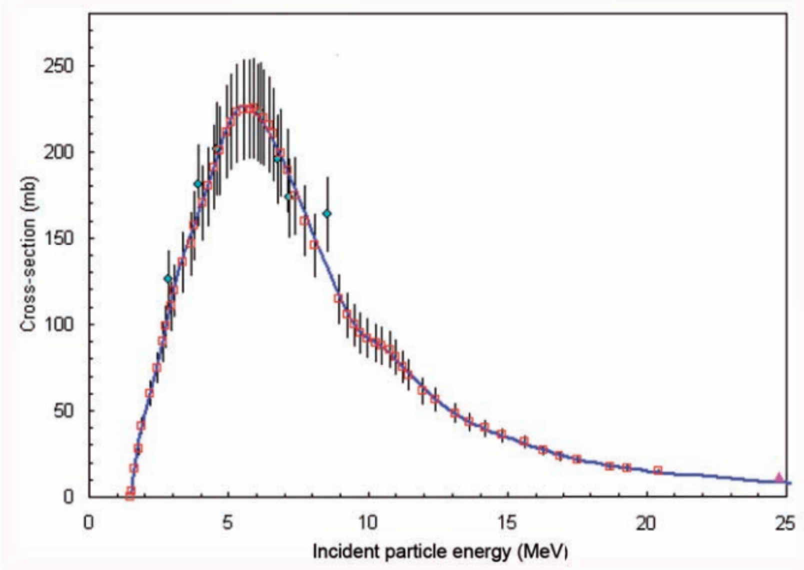

Fig. 1.4 Yield for the ^{20}Ne(d,α)^{18}F reaction pathway as a function of the energy dependence of the cross section [2].

This means the ^{18}F production yield will be much higher using a proton beam of 12 MeV on a thick target in comparison to deuterons with comparable energy of approximately 12 MeV as well [2]. The resultant ^{18}F is typically produced using ^{18}O-enriched water as the target material such that ^{18}F is produced as the fluoride ion in the target water and can be extracted.

Therefore, there are several factors to consider when producing radioisotopes such as the reaction channel used, the target nucleus, the energy to maximise yield and the form of the product. Other factors such as the optimising the specific activity and minimising radioisotopic impurities (contaminants) can then be analysed as well. The production of radionuclides can be expanded to developing radioactive tracers and radiopharmaceuticals as introduced below.

1.1.2 Radioactive tracers and radiopharmaceuticals

The use of radionuclides in the scientific and medical disciplines are commonly utilised in imaging, radiotherapy and radiotracers where radiotracers are required across all of these disciplines. Radiotracers consist of a chemical compound, having the role of a carrier, in which a radionuclide is bound and one or more atoms have been replaced by a radionuclide. Tracers are carefully designed such that they are able to interact with the system to be probed without perturbing the system. The most commonly used positron emitters are briefly summarised in Table 1.1.

Table 1.1 The most commonly used positron emitters with corresponding typical nuclear reactions used for their production [10].

Radionuclide	$t_{1/2}$ (min)	Decay mode	Reaction	Energy (MeV)
^{11}C	20.3	β^+	^{14}N(p,α)	11 - 17
^{13}N	9.97	β^+	^{16}O(p,α)	19
			^{13}C(p,n)	11
^{15}O	2.03	β^+	^{15}N(p,n)	11
			^{14}N(d,2n)	6
			^{16}O(p,pn)	> 26
^{18}F	110	β^+	^{18}O(p,n)	11 - 17
			^{nat}Ne(d,α)	8 - 14

The focus of this research are the positron emitting isotopes that have application in imaging due to spatial recollections in photon emission from annihilation. Nuclear medicine and imaging utilises the gamma photons emitted by certain radioisotopes such that detection is enabled. If these radioisotopes are attached to biologically active molecules, the resulting compounds are called radiopharmaceuticals. These radiopharmaceuticals are specially designed to interact biochemically such that it reaches the target site in the human body, for example for disease diagnosis or drug development.

One of the most commonly utilised positron emitting radiopharmaceuticals used is ^{18}F-fluorodeoxyglucose (^{18}F-FDG) [14], initially developed for mapping brain glucose metabolism in human neuroscience by researchers in collaboration from the National Institute of Health, the University of Pennsylvania and Brookhaven National Laboratory in 1976 [15]. Incorporating ^{18}F into FDG makes it analogous to glucose and can indicate levels of cellular metabolism, therefore allowing for the mapping of glucose in tissue.

Production of ^{18}F and synthesis of ^{18}F-FDG

^{18}F-FDG cannot be synthesised in a cyclotron as the glucose-complex will not withstand the bombardment. Therefore, ^{18}F-fluoride is first developed before being labelled and processed with the glucose-complex to complete the radiopharmaceutical tracer. The most common nuclear route used to produce ^{18}F worldwide is ^{18}O(p,n)^{18}F where naturally occurring and stable ^{18}O is used as the target and irradiated by a proton beam using a cyclotron. Two forms of ^{18}F can be produced; an aqueous solution of ^{18}F-fluoride ion is produced when the target is liquid $H_2^{18}O$ and ^{18}F-F_2 gas is produced when the target is $^{18}O_2$ gas [16].

Small volume ranging from 1 - 3 mL of ^{18}O enriched water (volume is dependent on the set up and apparatus used as well as minimising the quantity due to high cost of this isotope) is placed inside the designed target. The target is carefully designed and constructed to handle the heat consequent of the bombardment process. Majority of protons are lost to heating and only a small fraction of the protons are responsible for the production of ^{18}F [17]. The target is bombarded such that ^{18}O nucleus captures a proton and ejects a neutron. After the bombardment is complete the ^{18}F-fluoride ion solution is transferred remotely for safety precautions as a result of high radiation and then processed where the ^{18}F-fluoride ion is removed from solution and the ^{18}O-enriched water recovered.

Once ^{18}F is produced in a cyclotron as dissolved ^{18}F-fluoride ions in water, an automated process is necessary to rapidly synthesise ^{18}F-FDG particularly with ^{18}F's half-life of 110 minutes. As noted, the reactions ^{18}O(p,n)^{18}F or ^{20}Ne(d,α)^{18}F are commonly used to synthesise ^{18}F and produce ^{18}F-fluoride ions in water which is separated and extracted from solution via a "trap and release" process using an ion exchange column [17]. The column is eluted with an acetonitrile solution of 2,2,2-cryptand and potassium carbonate and eluates evaporated. This is then treated with mannose triflate and the fluoride anion displaces the triflate leaving group, resulting in fluorinated deoxyglucose [14]. In the final step base hydrolysis is implemented to remove the acetyl protecting groups after removing the cryptand. An overview of the scheme is shown in Fig. 1.5.

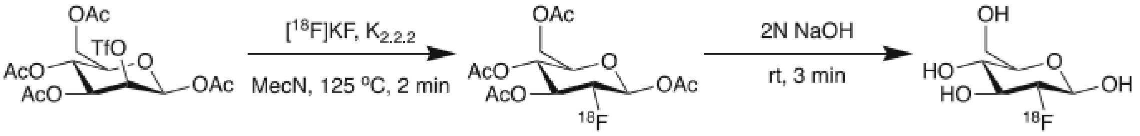

Fig. 1.5 Synthesis of ^{18}F-FDG by nucleophilic substitution. Once ^{18}F-fluoride ion in ^{18}O-enriched water is produced, it undergoes a separation and extraction process such that the ^{18}F-fluoride ion is converted into a potassium salt and water separated out. This then reacts with mannose triflate (left) and the produced unhydrolysed intermediate ^{18}F-FDG [14] undergoes hydrolysis and purification to form ^{18}F-FDG (right) [18].

Although ^{18}F-FDG was initially produced via electrophilic fluorination with ^{18}F-F$_2$ and is still a viable method, producing ^{18}F-fluoride ion in large quantities is more economical and supported via the high yielding ^{18}O(p,n)^{18}F reaction channel. The nucleophilic fluorination method described above also produces a higher yield of ^{18}F-FDG [14]. Radiotracers and radiopharamceuticals such as ^{18}F-FDG have proven to be beneficial for noninvasive molecular imaging and delivering therapeutic dose of ionising radiation based on their labelled medical radioisotopes. In particular, positron imaging continues to have a meaningful impact in medical and science disciplines. The cyclotron target where ^{18}O is bombarded is washed after irradiation with high purity water and produces up to 30 mCi of ^{18}F in water. Although it is not clinically compliant, this potential source of ^{18}F is typically easily accessible, more cost effective and suitable for this research. However, this mechanism was not available for the present work. In the context of this research, the access to this was limited and commercially available ^{18}F-FDG was used for all radiochemical experiments and developed for novel applications in physics and engineering.

1.2 Positron imaging considerations

Positron emission tomography (PET) is a well-established imaging technique which provides characterisation and visualisation on metabolic functions and receptor binding, and has a wide-range of medical applications in patient management such as staging and diagnosing (leading to treatment) various cancers, identifying coronary artery disease (CAD) and examination of neurological functions [19]. A PET scan displays the distribution of a positron-emitting tracer administered to a patient via injection of a chemical compound containing this positron-emitting isotope.

Once the radioactive tracer is injected into the subject, it embeds within the subject's metabolic process after equilibrating and travels to the targeted organs or tissues after a particular period of time [20]. The unstable radioisotope decays through β^+ decay during the metabolic process where the formed positrons travel only a few millimetres before colliding with the electrons of the neighbouring atoms in an annihilation process [19,20] where two 511 keV gamma photons are emitted approximately back-to-back. The isotopes used have relatively short half-lives (usually less than 2 hours) to allow for equilibrium in the body and avoiding prolonged exposure to radiation [21].

As shown in Fig. 1.6, the scintillation crystals surrounding the patient absorb and convert the high energy gamma photons into low energy visible photons.

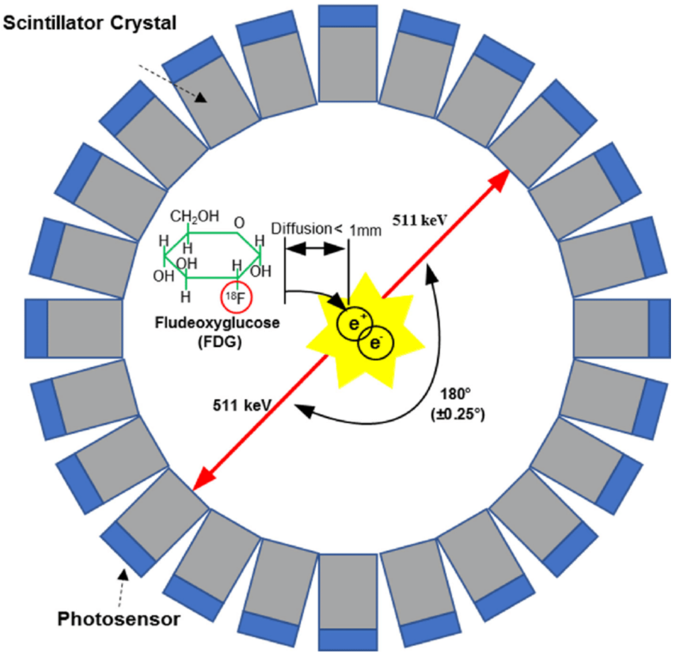

Fig. 1.6 Illustration of an annihilation event and a PET detector ring detecting the resulting pair of gamma photons (indicated by the red arrows) emitted by a ^{18}F-FDG tracer [20].

A photosensor is then used to convert light signal into an electrical signal such that a modular detector can be used to construct a detecting ring to record three electronic signals: the time when the gamma photon hits the detector, the position when the gamma photon hits the detector and the energy of the gamma photon [20]. These signals are processed such that distribution of gamma radiation allows construction of a three-dimensional image correlating to the spatial distribution of the radioisotope and hence uptake of the targeted radiopharmaceutical.

In the uptake of the radiopharmaceutical ^{18}F-FDG, regions of increased or decreased uptake reflect the rates of glucose metabolism as ^{18}F-FDG concentrates in cells that depend upon glucose as an energy source or whose dependence on glucose changes under pathophysiological conditions. For example, in the case of ^{18}F-FDG this uptake is equivalent to energy we use in our brain. As shown in Fig. 1.7, the difference in brain activities are measured by glucose usages and illustrated where yellow-to-red indicate higher brain activity, such as when patients generating words, whereas green-to-blue indicate lower brain activity [15]. A medical professional will analyse that there is additional brain activity in the schizophrenic brain. Among the few symptoms, schizophrenic patients typically exhibit symptoms of hallucinations, disorganised speech and/or thinking and abnormal motor behaviour. The development of PET has transformed clinical impact on patient care ranging from non-critical to life-threatening diseases.

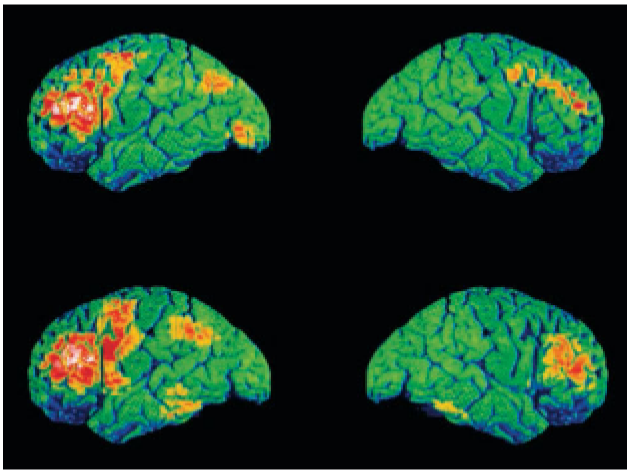

Fig. 1.7 Example of PET scans showing the difference in brains of a normal patient (top) and a schizophrenic patient (bottom) [15].

Although PET is proven to have a great impact in medical imaging by producing three-dimensional images of a tracer in a tracer, positron emission particle tracking (PEPT) allows for the location of the centroid of a single-point-positron emitting tracer particle moving in a system. In motivation to developing ^{18}F tracer particles for this research, an overview of PEPT technique which requires production of a suitable representative tracer particle, instrumentation, data processing and application is presented in conjunction with the requirements of successful PEPT tracking and representative data.

1.3 Positron emission particle tracking (PEPT): An extension of PET

PEPT is a non-invasive measurement technique used to measure the trajectory of a particle and applied to study systems of flow; for example multiphase systems such as rotating kilns and granulators with materials ranging from liquid, organic polymer to metallic and mineral particles. PEPT was devised in the late 1980s and techniques further developed in the early 1990s at the University of Birmingham where the first Positron Imaging Centre (PIC) was established, followed by the establishment of PEPT Cape Town at the National Research Foundation (NRF) accelerator facility iThemba LABS (Cape Town, South Africa) in 2009 [22].

In order for the PEPT technique to function, a radioisotope which undergoes β^+-decay has to be incorporated into a tracer particle such that the tracer emits positrons which annihilate with electrons and thus produce two 511 keV gamma photons which are emitted back-to-back i.e $180^\circ \pm 0.5^\circ$. These gamma photons emitted are then detected in coincidence within field-of-view of the PET scanner and a virtual line of response (LOR) defined, indicating an annihilation event has occurred. In principle only two LORs are necessary, however PEPT data is processed using an iterative algorithm developed at Birmingham University to account for corrupt events that may result from the detection of gamma rays after undergoing Compton scattering and detection of random coincidences or were not associated with the same annihilation event [7,22], therefore multiple LORs (100 - 1000 s) are used. If multiple coincidence events are detected by the PET scanner in a short time then the LORs converge on the instantaneous position and the location is calculated using an iterative minimisation technique as shown in Fig. 1.8.

The precision in locating the tracer particle is proportional to the inverse square root of the data rate, hence activity, with high activity tracer particles preferred for high resolution tracking. The precision for a given data acquisition rate scales as $1/\sqrt{\text{activity}}$. In Fig. 1.9 [24] a smooth trajectory of the particle motion is realised with tracer activity 600 μCi, however dynamic information is lost with reduced tracer activity of 30 μCi. For a location produced out of every 1000 detected LORs, for a recorded data (LOR) rate of 1 MHz the particle

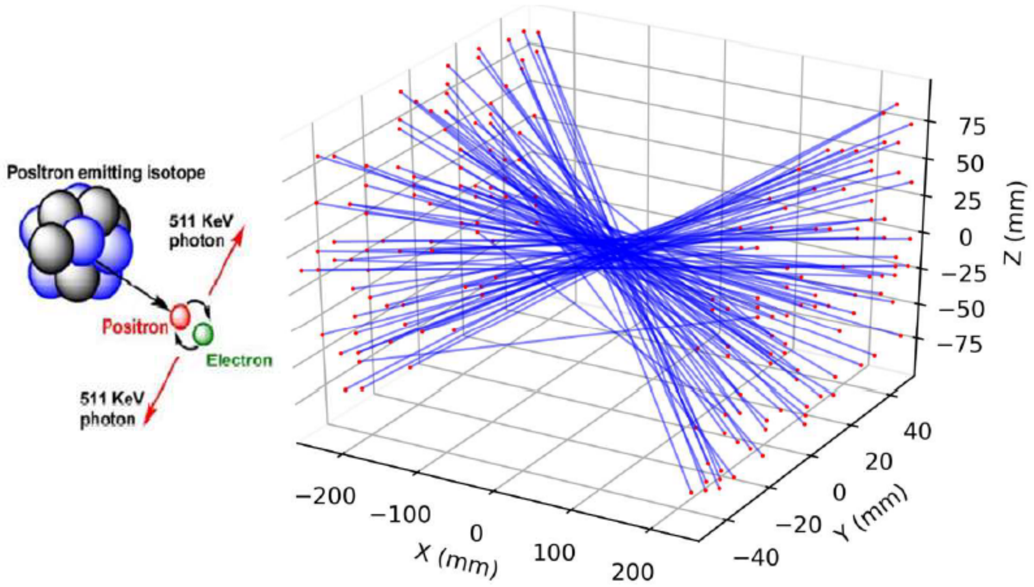

Fig. 1.8 Example measured LORs from a point source of positron activity. The majority of lines converge at the source position, forming the basis of the PEPT technique [23].

is located once per millisecond, i.e. at 1 kHz rate. Therefore, if it is moving at 1 ms^{-1} it will move 1 μm between locations which is smaller than the location precision. It is evident that higher data rates are preferred to resolve motion at higher speeds, accounting for tracer particle motion between locations. Attenuating materials also reduce the event rate detected for a given activity compared to that expected [25]. One or both photons may get absorbed before detection, thus lowering the recorded rate. Attenuation of one of the pairs and scattering or either/both can contribute to random coincidences increasing the noise fraction within the signal. Attenuation and scattering resulting in additional noise can be accounted for by increasing the activity of the tracer and changing the algorithm parameters to account for an increased fraction of corrupt data. It has been shown that tracer radioactivity ranging from 300 - 1000 μCi is sufficient for PEPT experiments [24].

As in selecting the correct pharmaceutical in medicine, in order for the PEPT data to be representative of the study, the tracer particles should be identical or near similar in both physical and chemical characteristics the the bulk of the system under study. This is motivated by the fact that the motion is dependent on factors such as the tracer particle size, density, shape and surface properties [24].

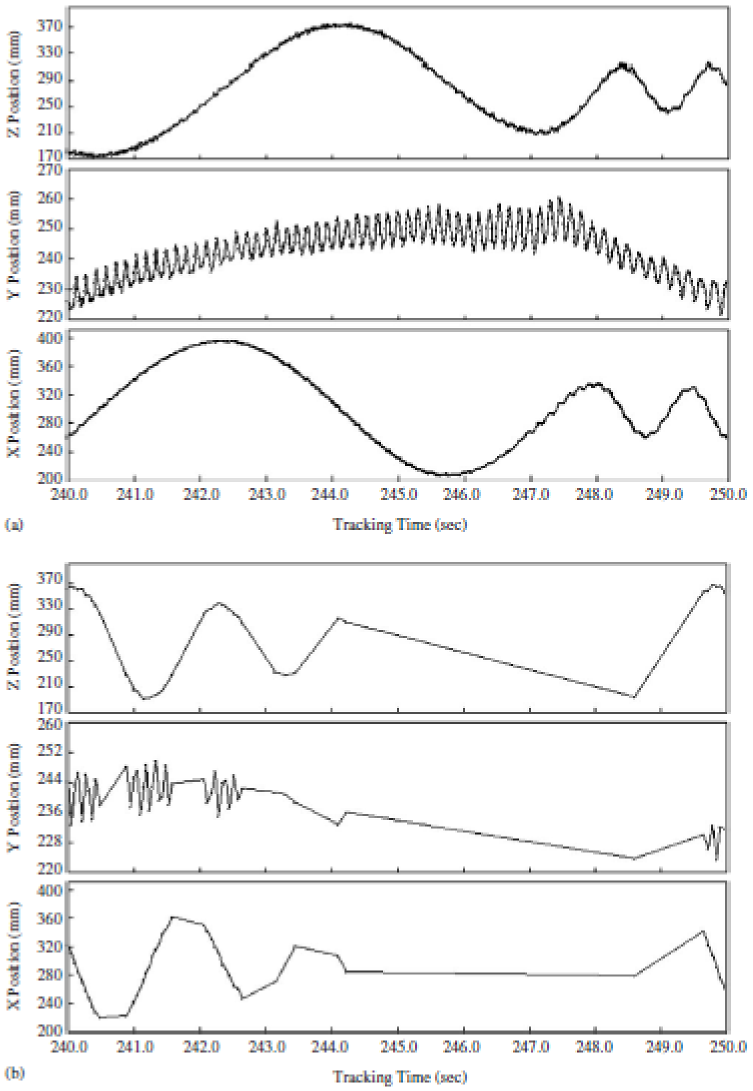

Fig. 1.9 Trajectory of a tracer particle with radioactivity (a) 600 μCi and (b) 30 μCi [24] showing that PEPT data precision decreases with decreasing tracer particle radioactivity.

1.3.1 The PEPT technique

As discussed, the PEPT technique relies on a tracer particle radiolabelled with a suitable positron emitting radionuclide that undergoes β^+-decay such that the positrons annihilate with surrounding electrons and produce back-to-back 511 keV gamma photon pairs. With the gamma-ray pairs detected in field-of-view of a PET scanner and resolution established, if both of these back-to-back gamma photon pairs are detected simultaneously (coincident with a 12 ns time window) then a LOR can be constructed. This LOR allows infers the origin of the annihilation event along this line. In principle only two LORs are necessary, however multiple LORs (100 - 1000s) are required as corrupt events may result from the detection of gamma rays after undergoing Compton scattering or random coincidences detected from a different annihilation event [7,22] as illustrated in Fig. 1.10.

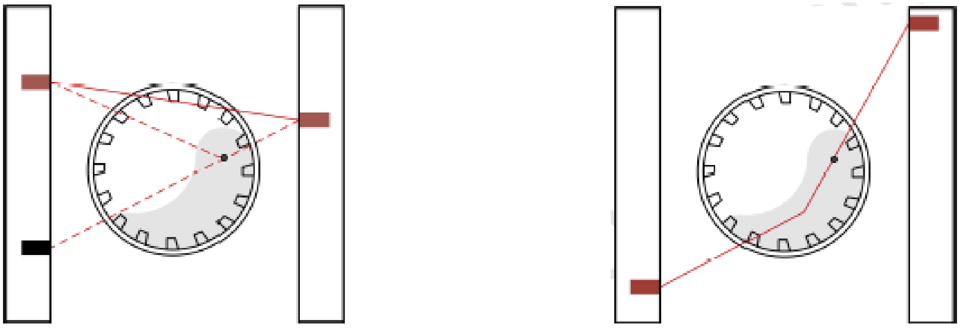

(a) Random (b) Scattered

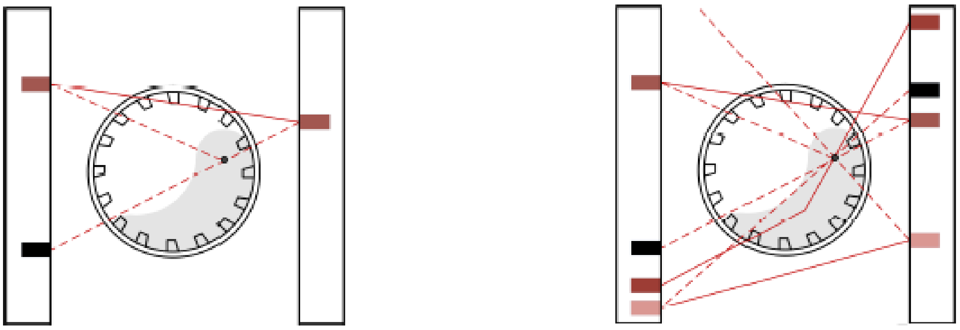

(c) Associated (d) Spurious

Fig. 1.10 Illustration of corrupt events that may result from the detection of: (a) random coincidences, (b) gamma rays after undergoing Compton scattering, (c) when an associated emitted gamma photon not related to its positron emission, or (d) a combination of all three [7].

If multiple coincidence events are detected by the PET scanner in a short time then the centroid of the LORs can be determined and the trajectory of the particle developed through an iterative location algorithm. The technique [26] involves binning LORs into time steps of the order 1 ms where an iterative algorithm is implemented to determine the tracer location by finding the set of LORs that minimises the sum of the perpendicular distances to the various LORs in each bin as shown in Fig. 1.11, with the corrupt LORs discarded and recalculated accordingly [27], and allows for the trajectory of the tracer particle to be built as outlined in Fig. 1.12.

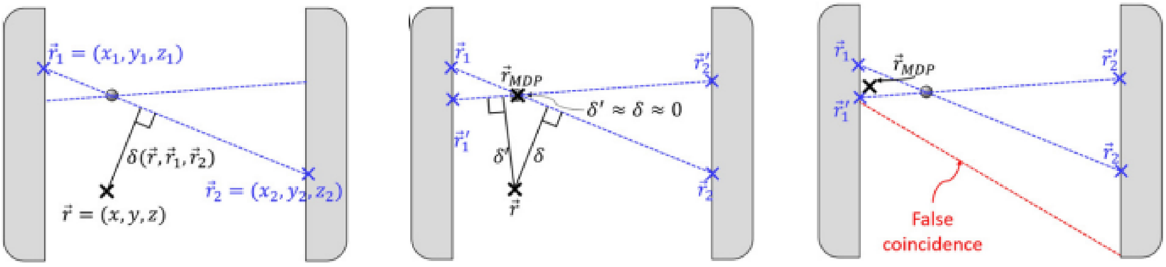

(a) (b) (c)

Fig. 1.11 (a) Illustration of the perpendicular distance, δ, between an LOR and arbitrary point *(x,y,z)* in space, (b) the minimum distance point (MPD) $\vec{r}_{MPD}$ corresponding to the point of intersection and (c) a false coincidence example showing deviation from the true particle center [28].

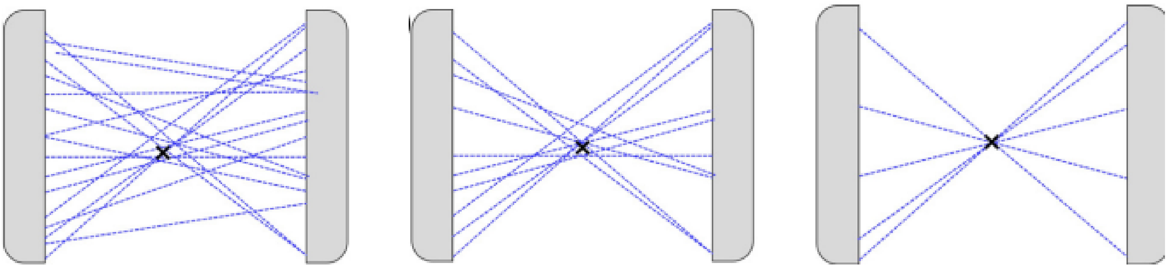

(a) (b) (c)

Fig. 1.12 (a) The PEPT technique begins with a set of measured LORs and (b) as recalculation occurs, (c) only a fraction of the original LORs remain to determine the centroid [28].

Given that an understanding of the PEPT technique and tracer requirements are built, another crucial aspect of the PEPT technique is the instrumentation used for measurements. In particular, focus will be on the instrumentation at PEPT Cape Town.

1.3.2 PEPT instrumentation

Development of PEPT at the PIC at the University of Birmingham

The PEPT technique was developed in the early 1980s [29], followed by further development where the original Birmingham Positron Camera was built and replaced with the Forte PET camera just before 2000. The Forte PET camera has two heads with dimensions 500 × 400 mm^2 and 16 mm thick, each with a single crystal of thallium-activated sodium iodide (NaI(Tl)) scintillator.

The Forte PET camera was an improvement in comparison to the original Birmingham positron camera which had low quantum efficiency for detecting 511 keV energy level photon annihilation. The Forte PET camera has the capability to track a tracer particle with speed at 1 ms^{-1} to within 0.5 mm approximately 250 times per second. The heads are optically coupled to an array of 55 photomultiplier tubes, each channeled through a separate analogue-to-digital converter [30]. Using the ADAC Forte camera, a tracer can be tracked in field-of-view of the detector with dimensions $80 \times 50 \times 40$ cm^3, however tracking is limited near the edges of the specification boundaries. The heads are conveniently mounted with a motorised drive such that rotation about a horizontal axis is allowed. Adjustment of the face-to-face separation of the detectors range from 250 to 800 mm [22]. It was found that this camera offered spatial resolution and sensitivity improvement by 25% and factor of 10 respectively. With the resolving time also reduced to 60%, this improved data rates and overall enabled the tracking of faster particles with improvement in the precision of location.

Unfortunately the ADAC Forte camera provided restriction of the system under study based with respect to geometry and sizing. Therefore, a newer Modular Positron camera was developed which allows for arrangement in multiple varying geometries. This comprises of bismuth germinate (BGO) detectors where they are grouped into modules. Each bucket has its own analogue to digital converter (ADC), preamplifiers and four detectors. The Modular Positron camera houses 16 buckets which is connected to a data processing system which identifies coincidence events and data recorded. In addition to the advantageous flexible geometry, the Modular Positron camera is able to deliver high data rates, however the effective count rate is limited by the speed of storing data from the PET camera.

Development of PEPT Cape Town

PEPT Cape Town is conveniently situated at NRF-iThemba LABS, Faure, South Africa and opened in 2009. NRF-iThemba LABS houses a 200 MeV SSC, capable of accelerating protons to energies of 200 MeV and heavier particles to high energies. There are also two injector cyclotrons, namely a 3 MV Tandetron and $k = 11$ cyclotron, producing beams of light ions and polarised light or heavy ions respectively [22]. These cyclotrons are typically utilised for ion beam analysis and the 11 MeV cyclotron is used to produce ^{18}F-FDG which is utilised commercially for medical imaging and provided to local medical facilities. The facilities at NRF-iThemba LABS produces attractive resources for radioisotope production, radiotherapy and nuclear and applied physics research, thus assisting in particular for our radionuclide production requirements.

PEPT Cape Town is the second operational PEPT facility in the world and houses an ECAT "EXACT 3D" HR++ (Model: CTI/Siemens 966) PET camera, shown in Fig. 1.13 [22], which was originally designed with the aim of achieving high sensitivity and high efficiency for clinical PET-based research used at Hammersmith Hospital in the UK from 1995 until it was decommissioned.

Fig. 1.13 The Siemens ECAT "EXACT3D HR++" PET scanner, commonly referred to as HR++, used at PEPT Cape Town [31].

The camera consists of 48 rings of standard bismuth germinate detector elements arranged cylindrically (each detector having dimensions 4.39 mm transaxial × 4.05 mm axial × 30 mm deep, grouped in blocks of 8 × 8) with a ring diameter of 82 cm and axial length of 23.4 cm [22,32]. The data acquisition system can maintain a maximum acquisition rate of about 4 million coincidence events per second, and the mean spatial resolution of the scanner for PET imaging was 4.8 mm (transaxial, 1 cm off-axis) and 5.6 mm (axial, on-axis) [22] as the defined width of the distribution equivalent to half the maximum ordinate of the peak. For a stationary tracer at the centre of the field of view of the scanner, the uncertainty in the measured positions is about 1 mm and this increases as the speed of the tracer increases. Tracers moving at speeds up to 15 ms^{-1} have been successfully tracked with PEPT [31].

The limitation of the camera remains its geometry of its field-of-view as configuration makes access for the system of study to the apparatus difficult as well as the area of imaging. However, PEPT Cape Town also houses an ADAC Vertex model, as shown in Fig. 1.14, with two parallel and adjustable heads and offers a field-of-view of 380 $\times$ 500 $\times$ 300-800 mm^3.

In aid of producing tracers at PEPT Cape Town, a modular tracer laboratory for radiolabelling tracers is also available and being accommodated to incorporate further tracer developments. The laboratory is conveniently set up near the instrumentation operations and

Fig. 1.14 PEPT Cape Town's second camera, the ADAC Vertex model with two parallel heads [31].

houses experimental requirements such basic chemical laboratory apparatus, fumehoods, lead shielding blocks to minimise exposure to harmful radiation and more. It is worthy to note that PEPT Cape Town expands to the Department of Physics at the University of Cape Town (UCT) where development of hardware takes place in the electronics laboratory and mechanical workshop.

PEPT offers applications in various disciplines such as mineral processing, petroleum geology, and flotation where typically dynamic information can be analysed to investigate the behaviour and characteristics of multiphase systems. As an example of the analysis of PEPT measurements, the tracer occupancy (where the particle spends the amount of time the particle spent at each location) can be realised from the coordinates as shown in Fig. 1.15. The segregation and distribution can be maximised in a system [33], as well as further parameters investigated such as increasing the rotation speed, varying bead ratios and/or the material itself.

Subsequently the dynamic characteristics can be analysed using PEPT data of the system such that various physical processes such as segregation, mixing and flow patterns can be modeled. For example, it is possible to obtain the time differential of the tracer particle trajectory to determine the velocity fields. An example of the average velocity field plots are shown in Fig. 1.16.

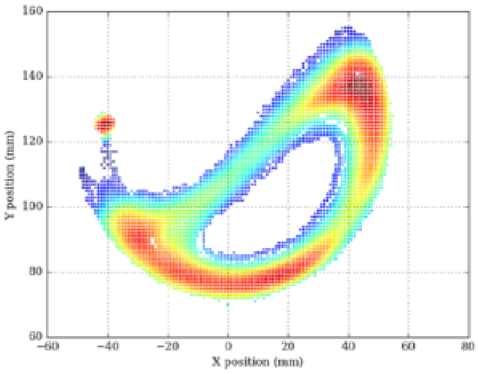

(a) (b)

Fig. 1.15 The tracer occupancy of (a) 5 mm and (b) 3 mm particles in a rotating cylinder can be realised. Here the colour relates to the occupancy with red indicating the highest occupancy [31].

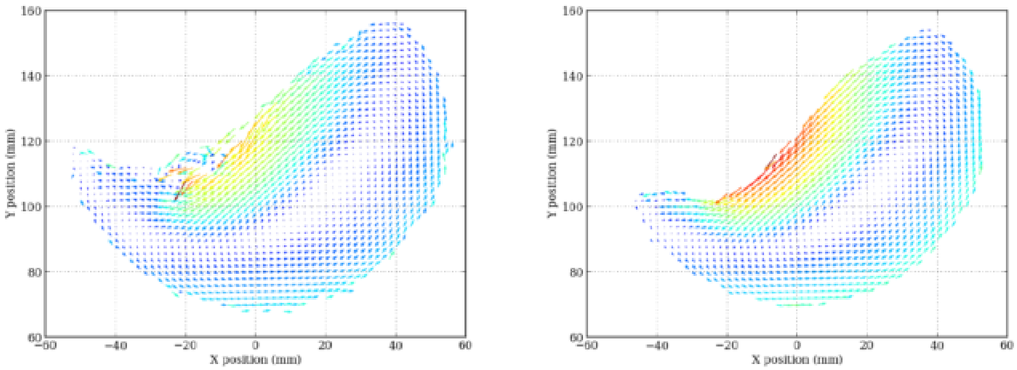

(a) (b)

Fig. 1.16 The average velocity field plots of (a) 3 mm and (b) 5 mm tracer particles in a rotating cylinder. Here the colour relates to the occupancy with red indicating the highest velocity [31].

Given that the requirements of successful PEPT tracking is well understood, in addition to the technique and application, a primary component of the PEPT technique is the development of suitable tracers. The nature of radioisotopes proves to be the primary component in developing tracers and its use in PEPT tracking, together with applications and instrumentation required, impactful. At PEPT Cape Town ^{68}Ga radiolabelling techniques is well established and the aim is to extend the tracer development menu to the advantageous ^{18}F based tracers using chemical sorption techniques.

Chapter 2

PEPT Tracer Development

There are many radioisotopes used for radiolabelling for various fields of study, however PEPT requires a radioisotopes that decay by positron emission with an ideal half-life that allows for detection for the typical duration of a PEPT experiment, but not too long to avoid prolonged radiation exposure and harmful waste. Examples of suitable radionuclides include ^{18}F, ^{68}Ga and ^{64}Cu, however ^{18}F-based tracer particles are particularly ideal for PEPT because ^{18}F has a half-life of 110 minutes which is suitable for PEPT experimental timescales. Advantageously ^{18}F is a pure β^+ emitter with no additional gamma emissions, thus its use intrinsically increases the signal to noise ratio in PEPT studies. Spatial resolution is also improved with shorter positron range.

2.1 Historical overview of radioisotopes used in PEPT

The radioisotopes used at the PIC at Birmingham University are ^{18}F, ^{66}Ga, ^{22}Na, ^{61}Cu and ^{64}Cu, with ^{18}F most frequently utilised. ^{18}F is produced in the MC40 Cyclotron using the ion beam ^{3}He via reactions ^{16}O(^{3}He, p)^{18}F and ^{16}O(^{3}He, n)^{18}Ne $\rightarrow$ ^{18}F, where purified water or solid targets are under bombardment of the 33 MeV ^{3}He beam. In the process oxygen is converted to radioactive fluorine. A 20 minute "cool down" period is implemented after the bombardment to allow for short-lived isotopes to decay. If bombarded on solid materials then the ^{18}F produced will be chemically bound to structural elements of the solid material, and if bombarded on purified water then the ^{18}F produced will be in ionic state. Before the bombardment the water is purified by distillation and de-ionised such that it has a resistance of 18.2 MΩcm and surface tension of 72.8 m/Nm (once the resistivity drops there are too many free ions/radicals/other species and the labelling becomes less efficient). A designed titanium or silver target holds this purified water where it will be bombarded by the 33 MeV

^{3}He beam at a current of 10 μA for 120 minutes. A yield of 15 - 18 mCi/mL is typically achieved [24].

Since the late 1980s, NRF-iThemba LABS has been known for supplying high quality accelerator-based radiopharmaceuticals and radiochemicals, including short-lived single-photon emission computerised tomography (SPECT) radiopharmaceuticals, to over 40 nuclear medicine departments in South Africa private and public hospitals. In 2006, the first commercial PET radiopharmaceutical, ^{18}F-FDG, and in 2008 the first commercial ^{68}Ge/^{68}Ga generator was produced by NRF-iThemba LABS. Since the late 1990's, the supply of long-lived radiochemicals focused mainly on the export of ^{22}Na solution and ultra-high vacuum ^{22}Na positron sources and unprocessed radiochemicals such as irradiated Rb metal targets [33].

The radioisotope commonly used at PEPT Cape Town is currently ^{68}Ga, eluted from a ^{68}Ge/^{68}Ga generator provided by NRF-iThemba LABS using 5 mL of 0.6 M hydrochloric acid (HCl). It has a half-life of 68 minutes which is sufficient for the duration of PEPT experiments and does not pose prolonged exposure to radiation. The generator has a small column packed with treated SnO_2 which is loaded with ^{68}Ge and decays to ^{68}Ga by electron capture [35]. Chelex 100 and and Purolite NRW100 are the typical resins used where the sorption of ^{68}Ga is dependent on the HCl concentration, ^{68}Ga concentration and shaking time [36].

2.2 Tracer fabrication for PEPT

PEPT tracers have all activity concentrated into a single point, therefore high efficiency in attaching radioactive material to a single point rather than a distributed bed is required. PEPT tracers are much lower in activity in comparison to conventional PET tracers, however the specific activity of PEPT tracers is much higher at the location of the particle. This volumetric concentration is a significant challenge in PEPT tracer production.

Various methods have been developed to radiolabel a tracer particle, namely direct activation and chemical sorption, with chemical sorption comprising of ion exchange and surface modification as summarised in Table 2.1 and detailed below [23].

Table 2.1 Overview of the PEPT tracer radiolabelling techniques. The direct activation material used matches the bulk whereas the ion exchange materials typically have to undergo treatment to match the bulk density.

	Direct Activation	Ion Exchange	Surface Modification
Typical activity (μCi)	2600	800 - 1000	± 600
Typical size range (μm)	> 1000	50 - 1200	100 - 1000
Typical material	contain oxides	ion exchange resin	reacts with radioisotope

2.2.1 Direct activation

Direct activation is used to produce tracer particles with a diameter greater than 1 mm and involves bombardment of the tracer particles using appropriate reaction chains and beams; for example the PIC at Birmingham produces ^{18}F tracer particles via direct activation by bombarding the ^{16}O-based tracer particles with a 33 MeV ^{3}He beam where ^{16}O is transformed to ^{18}F, deposited as a structural element within a layer approximately 0.3 mm deep, following the nuclear reaction of $^{16}O(^{3}He,p)^{18}F$ or $^{16}O(^{3}He,n)^{18}F$. In addition to the materials being oxygen bearing and greater than 1 mm in diameter, the labelled materials must withstand the high temperature produced during bombardment. The consequential isotopes that are produced from nuclear reactions with structural elements of the tracer particles decay rapidly due to their short lives [24], leaving the relatively longer lived ^{18}F for practical applications.

At PEPT Cape Town previous experiments developing tracer particles via the $^{16}O(\alpha,pn)^{18}F$ nuclear reaction was established [37] as depicted in Fig. 2.1.

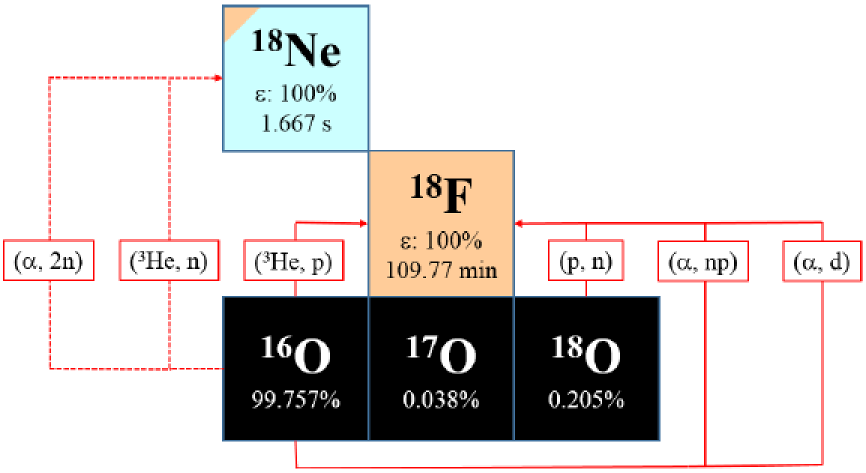

Fig. 2.1 Typical reaction pathways for ^{18}F production from oxygen targets, using proton, ^{3}He and alpha particle beams. Many competing reactions contribute to the ^{18}F end-product, sometimes through intermediate short lived stages [23].

Silicon dioxide (SiO_2) glass tracer particles (^{16}O bearing targets) were placed in an aluminium target holder, housed in the "Elephant" target station and bombarded with a 100 MeV alpha particle beam using the Light-ion solid-pole injector cyclotron (SPC2) and Separated Sector Cyclotron (SSC) as shown in Fig. 2.2.

The glass beads were placed in a capsule prior to being housed in the target holder designed such that it had a perforated aluminium lid and enclosure [38,39] to allow for active water cooling. The water circulating allows the glass beads to rotate but whilst still being housed in its capsule. The rotation encourages adequate heat distribution and a uniform activation surface area.

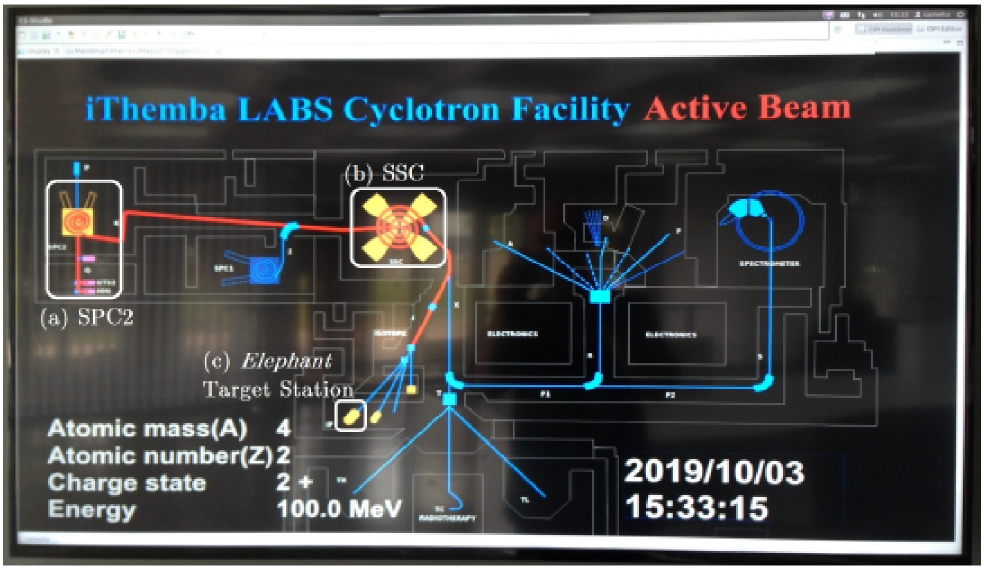

Atomic mass(A) 4
Atomic number(Z) 2
Charge state 2 +
Energy 100.0 MeV
2019/10/03
15:33:15

Fig. 2.2 Depiction of the beam path where (a) ^4He ions are axially injected to the SPC2 injector and accelerated to approximately 10 MeV energies. (b) The SSC then accelerates the beam to 100 MeV and magnets focus the beam in to a circular sweep which then (c) travels to the "Elephant" target stations where the aluminium target holder houses 10 silicon dioxide glass beads of diameter 5 - 10 mm [38].

The target stack and beam entry is illustrated in Fig. 2.3. The alpha beam averaged approximately 1 μA over approximately 2 hours of bombardment on the targets with fluctuations of 0.2 μA during bombardment where the beam first passes through a vacuum line and there is a cooling foil window which allows for border between the vacuum and water cooling layer, such that the beam then travels through the cooling water layer and glass capsule lid to reach the targets.

The beam undergoes various energy losses and spread as well as loss in beam current due to scatter and absorption due to interaction with the material [38].

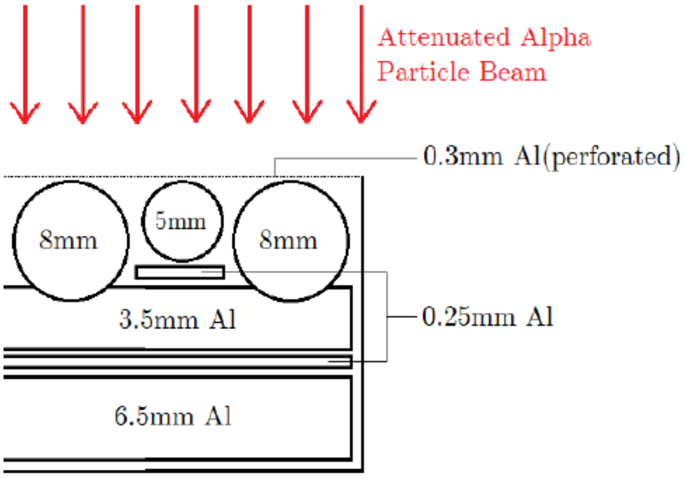

Fig. 2.3 Schematic of the alpha beam travelling and irradiated the glass bead capsule [38].

As shown in Fig. 2.4, radioisotope activation yields were characterised by half-life measurements and gamma photon spectroscopy, with the highest yield being < 3 mCi of ^{18}F on a single glass sphere [39,40]. Few impurities from other nuclear reaction channels were observed.

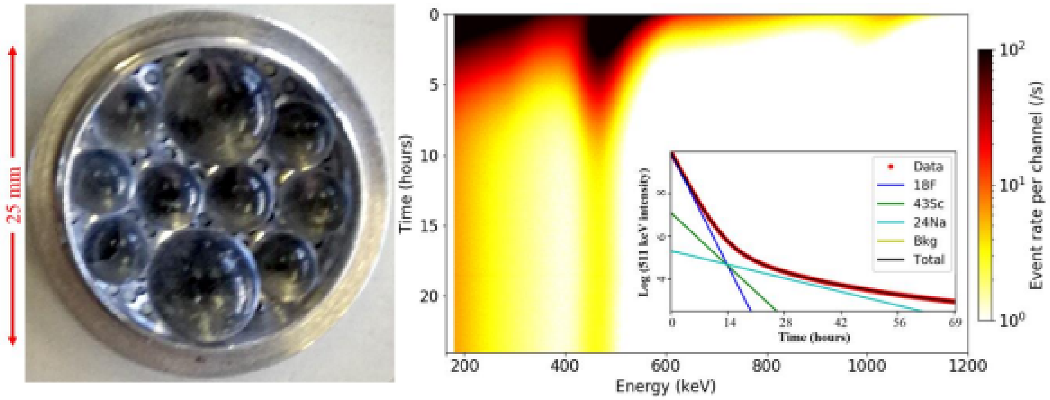

Fig. 2.4 Left: target holder with SiO_2 glass beads of 5 – 10 mm diameter. Right: time-series spectroscopy recorded over 24 hours (vertical axis) showing the principle 511 keV photopeak from positron annihilation, there are very little contaminant species at other gamma energies. The inset shows the 511 keV peak area decaying over time, fitted to half-lives of ^{18}F and the theorised contaminants. These data are consistent with over 95% of the produced activity being due to ^{18}F [23,38,39].

2.2.2 Ion exchange

Ion exchange techniques are utilised to produce resin tracers with diameters $< 1000\ \mu$m and when suitable oxygen bearing substances or materials are not available. The technique involves using a sorbent resin to control the uptake of the appropriate radionuclide. These resins consist of small porous beads with functional groups attached to the styrene divinylbenzene (DVB) copolymer lattice [41]. Each resin structure has a fixed ion and counterion such that electrical neutrality is preserved. This counterions are mobile, therefore the counterions attached to the functional groups on the resin surface can be exchanged by introduced ions. The two types of resins are cation and anion resins, where positive ions are attracted to cations and negative ions are attracted to anions.

In order for the exchange process to occur, the radioactive ions must have a higher affinity for the resin than the counterions. As shown in Fig. 2.5, the functional groups for anion resins are quaternary ammonium cations as N^+R_3 where R is the organic backbone and the mobile counterions in the anion resin beads are chloride anions. The resin is used in an ionic form with a lower selectivity for the functional group than the sample ions to be exchanged, where only ions of the same electrical sign are exchanged. The ion exchange process normally happens in aqueous solution, and here with $^{18}F^-$ ions dissolved in solution.

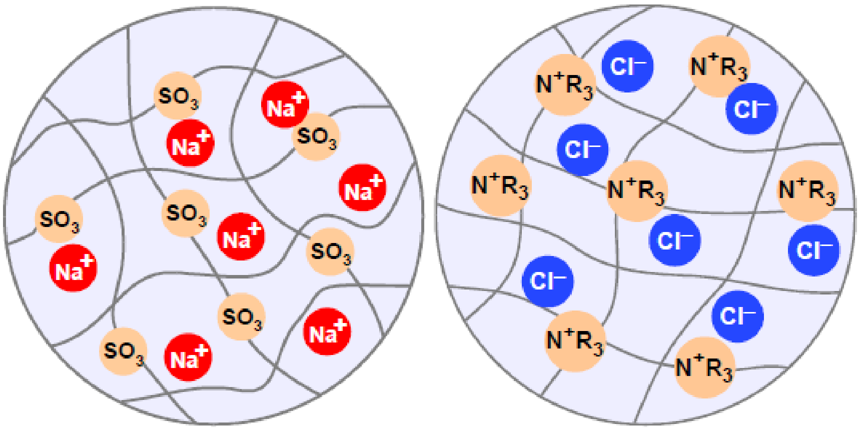

Fig. 2.5 Left: structure of a cation resin bead where the fixed ions are sulphonate (SO_3^-) and the mobile counterions are sodium (Na^+). Right: anion resin bead having similar structure to the cation resin bead but the functional groups are quaternary ammonium cations (N^+R_3) and mobile counterions are chloride anions (Cl^-), thus anion resins are suitable for ^{18}F radiochemistry development where chloride ions can be exchanged by $^{18}F^-$ ions. In the ion exchange process the electrical neutrality has to be preserved [42].

The uptake of $^{18}F^-$ on weak-base anion exchange resins is strongly controlled by water pH. The freebase amines in the weak-base anion exchange resins, eg. $RCH_2N(CH_3)_2$, interact with water and form $RCH_2N(CH_3)_2^+OH^-$ in which the OH^- acts as a counter ion and can be exchanged by $^{18}F^-$. The dissociation of the hydroxide ions from the functional group is very weak. As the process progresses, the hydroxyl concentration increases in solution causing the resin to convert back to the undissociated free-base form and inhibiting the anion exchange capacity. The affinity of $^{18}F^-$ ions to weak-base anion exchange resin is much weaker than hydroxide ions. Therefore, the use of weak-base anion exchange resins are limited as ^{18}F absorption can only perform at a low pH [23,24]. Alternatively, strong-base anion exchange resins are less affected by water pH or hydroxide ions since the affinity of $^{18}F^-$ ions is stronger than hydroxide ions of resins. The strong-base anion exchange resins used are quaternary ammonium derivatives in chloride form: R-$CH_2N(CH_3)_3^+Cl^-$, where chloride is the counter ion. However, because the affinity of the $^{18}F^-$ ion to the functional groups is much weaker than the Cl^- ion, the resin particles must first be converted into fluoride or hydroxide form e.g. R-$CH_2N(CH_3)_3^+F^-$, such that the converted F^- ions act as counter ions that exchange with $^{18}F^-$ ions as illustrated in Fig. 2.6. The scheme is shown in Eq. 2.1 and 2.2.

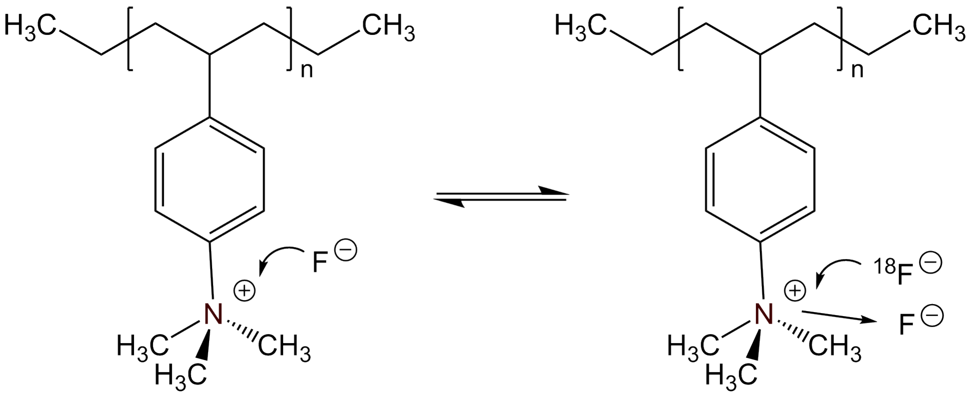

Fig. 2.6 Schematic representation of strong-base anion exchange resin (resin converted from chloride to fluoride form prior to radiolabelling), followed by F^- ion exchange with $^{18}F^-$ in an anion resin bead to gain radioactive uptake. An interchange of the isotopic label occurs where only a small percentage of F^- are exchanged with $^{18}F^-$.

$$\text{R-CH}_2\text{N(CH}_3)_3^+\text{Cl}^- + \text{K}^+\text{F}^- \leftrightarrow \text{R-CH}_2\text{N(CH}_3)_3^+\text{F}^- + \text{K}^+\text{Cl}^- \tag{2.1}$$

$$\text{R-CH}_2\text{N(CH}_3)_3^+\text{F}^- + {}^{18}\text{F}^- \leftrightarrow \text{R-CH}_2\text{N(CH}_3)_3^{+\,18}\text{F}^- + \text{F}^- \tag{2.2}$$

In developing ^{18}F tracer particles for PEPT Cape Town via ion exchange techniques, strong-base anion exchange resins Purolite A200 and A870 are ideal. When selecting resins for radiolabelling, chemical and physical properties, stability and reactive functional groups are all of importance. When analysing bead pore size, a defining factor is the resin crosslinkage that dictates the functionalised portion of the resin in relation to the water phase (the driver of ionic diffusion) and therefore influences various factors. Notably a higher crosslinkage resin has a lower moisture content and offers a more chemically and physically damage resistant structure [35,41]. Although higher crosslinkage resins offer higher total capacity, slower kinetic results in a lower operating capacity. In comparison, the lower the crosslinkage resins have more moisture content, a more porous structure and provide better kinetics. Lower crosslinkage resins are particularly useful for sorption of high molecular weight substances whereas higher crosslinkage resins are ideal for separation and sorption of low molecular weight inorganic anions [41]. However, resins are commonly utilised commercially on an industrial scale. In PEPT these resins are used to provide optimised exchange for a radioactive ion onto a single particle, therefore high exchange per particle is preferred to lower exchange per unit mass of resin.

Majority of anion exchange resins are commercially sized, purified and provided in chloride form but may be provided in other forms as well. In order to evaluate which form will provide more use in application, the order of selectivity is often useful and conversions to other forms are possible where the resin is typically utilised in a form with a lower selectivity for the functional group than the radioactive ions to be exchanged. In addition to the lower selectivity of the counterion being optimal for ion exchange, the selectivity can also provide insight into the quantity of introduced ion required if converting a resin form. To convert a resin to a form with a higher selectivity, 2-5 bed volumes of a 1 M solution of the counterion is required, whereas if the resin needs to be converted to a form with a lower selectivity, 1 bed volume of 1 M solution of the counterion is required relative to the difference in relative selectivity [41]. Intermediate conversions steps to obtain the desired form is also possible.

The resin ionic forms particularly vary in capacity, moisture and density. For example, a resin could vary in capacity as a result of resin swelling, however the number of active sites does not change. When a resin swells then the density of the active groups decreases and the volume capacity is essentially a measure of this active group density. In order to characterise the number of exchangeable monovalent ions a resin has, the total capacity expresses the number of active groups, however in actuality this total capacity is never reached. The operating capacity provides the characteristic of the reactive sites in the ion exchange process.

Both capacities can be expressed in equivalents per litre (mEq/L) or equivalents per gramme (mEq/g) of wet resin and dried resin respectively.

The relationship of resin volume vs. mass absorbed can be determined as well. A given percentage of a resin is cross-linked where every DVB cross-linking molecule can have an active exchange site. Theoretically (considering every DVB has a functional group) the number of sites can be related to the mass of the resin. For example for 8% cross-linking equates to adding 8% of DVB to 92% of polystyrene; 1 g has 0.08 g of DVB. The number of moles will be equal to the number of exchange sites, hence in equivalents.

The resin bead size can be determined as the volume is expressed as

$$V = \frac{4}{3}\pi r^3, \tag{2.3}$$

where r is the radius of the resin bead and can be determined from the diameter of the resin bead. However, in actuality this relation never holds true as the pore size related to the DVB may inhibit ion exchange or the DVB sites may not physically accept a functional group. Swelling and shrinking during the exchange process could also possibly change the size of the resin and affects the capacity due to restriction of some pores availability for ion exchange. In resin production the cross-linkage could also not correctly reflect the bound DVB.

Resins are offered in a range of particle sizes, however in order to compare radioactivity uptake effectively a comparable and narrow size distribution range selection is crucial. The resin size selected is strongly dependent on the application required. Fine resins offer a higher capacity and faster exchange rate whereas coarse resins have slower kinetics and offer lower operating capacity.

Purolite's strong base anion resins [43] are ion exchange resins based on a polystyrenic or polyacrylic matrix with either gel and macroporous structures. These include several characteristics such as Type I and Type II as well as mixed base and ion selective functionality. Type I resins have higher silica removal efficiency (ideal for industrial processes) and are thermally more stable, while Type II have a higher operating capacity. Polystyrenic resins are more rigid and more hydrophobic compared to polyacrylic based resins. They also typically have higher thermal stability. Generally, gel resins have a higher breaking weight and offer higher working capacity. Owning to their pores, macroporous resins have better resistance to physical stress and better access to the active sites [43].

Purolite A200 is a strong base anion exchanger, in particular a Type II, gel resin with polystyrenic structure. It has ionic form of Cl^- with total volume capacity of 1.3 eq/L. The A200 resin has high capacity and primarily used in the production of demineralised dealkalised water and dealkalised chloride as well as offering good silica, acid, and alkalanity removal in industry. The resin produces good kinetic performance and high regeneration efficiency if needed.

Purolite A870 is a dual functionality, gel resin with a polyacrylic structure. It has ionic form of Cl^-/free base with total volume capacity of 1.25 eq/L. The A870 is a unique bifunctional resin combining weak and strong base sites on the same beads, offering the highest operating capacity thus making it the most attractive resin to use for uptaking ^{18}F in this research. The A870 resin is typically used as an acid remover as well as natural organic matter remover in industry [43].

Although ion exchange resins are typically used on an industrial scale as described above, emphasis is on using single ion exchange resins for PEPT tracer development using sorption techniques. It is of importance that tracers produced are representative of the particles in the system of study, consequently PEPT Cape Town has developed several novel techniques to meet this requirement.

Making representative tracer particles

Using ion exchange techniques, the tracers produced are typically not representative of the particles of interest in the system of study as they consist of a polymer matrix which may not reflect the bulk behavior of the tracer particles [36]. Therefore, there are two methods employed to overcome this challenge and ensure that tracer properties are suitable; the coating method and the "drill and fill" method.

The coating method involves coating the ion exchange resin after radiolabelling to modify the surface or density properties with a coating [44]. The "drill and fill" method involves drilling a hole to the centroid of a bulk particle of interest and filling the hole with positron-emitting radionuclide, followed by sealing with an epoxy. The "drill and fill" method requires the particle be large and stable to prevent any damage during the process, however it is a viable alternative where it can be employed in applications without access accelerators. The direct activation method is not readily accessible, therefore the "drill and fill" method is typically used at PEPT Cape Town to develop tracers > 1 mm in diameter. Consequently, chemical sorption (in particular ion exchange techniques) is currently the motivated and advantageous method in producing ^{18}F tracer particles in this research. An overview of PEPT Cape Town tracers is illustrated in Fig. 2.7.

Fig. 2.7 A selection of PEPT Cape Town tracer particles from left to right: moulded, density modified, mineral coating, silica coating, coal particle, glass bead with ion-exchange inset. The images have a global scale with the tracer on the far left approximately 300 μm in diameter, up to 1 mm diameter on the far right [23].

2.2.3 Surface modification

Chemical sorption also comprises of surface modification and relies on adsorption of the radionuclide onto selective surfaces which allows certain materials selected to be extended and studied further with respect to their properties in order to improve selective adsorption of the radionuclide [45-47]. Although this method is not typically utilised, it is still of great interest and was developed at the PIC at the University of Birmingham and relies on altering surface chemistry of a particle before attempting to radiolabel. The objective is to enhance labelling efficiency and/or prevent activity leaching.

Surface modification can be done via chemical activation using metallic ions; they serve as active sites when on the solid surfaces such that anions bind to these metallic ions. This allows the uptake of ^{18}F onto solid surfaces to be investigated over a range of materials and optimise conditions. For example, in studies [45] as shown in Fig. 2.8, the radioactivity adsorbed in a single particle increased from 67 to 600 μCi for hydroxyapatite, increased from 2 to 400 μCi for quartz and from 2 to 152 μCi for polyethylene. The resin material still produced the highest uptake of ^{18}F.

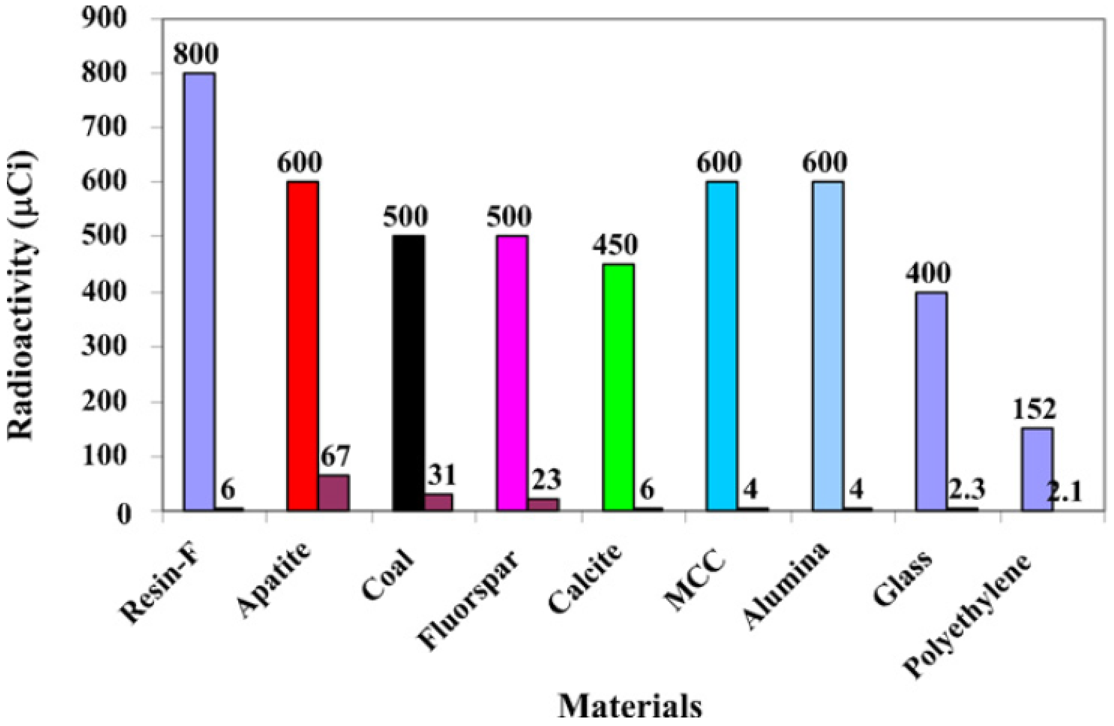

Fig. 2.8 Radioactivity uptake on a single particle under controlled conditions and optimum conditions (shown on the left and right for each material respectively) with size range of 212 - 250 μm [45,46].

It is likely that the adsorbed metallic ions alter the surface charges of certain solids or act as bridges, allowing for greater adsorption of ^{18}F and/or the adsorbed metallic ions could enhance adsorption of hydroxides which are then exchanged with ^{18}F in proportion to provide greater radiolabelling [45].

Although PEPT users are not perturbed by how the tracer is produced, what is important is that the resultant tracer is representative. The tracer developed needs to meet the specifications required for optimum tracking and the method chosen to represent a given a particle type will be that which is advantageous for that process.

2.3 Purpose of the study

The purpose of this research is the novel development of the specific tracer particle production mechanisms using ^{18}F and establish repeatable production of 50 - 1000 μm in diameter tracers with sufficient radioactivity to ensure that the measured PEPT data is reflective of the motion, irrespective of the tracer size and physical properties. Although the detection of tracer particles is limited by the scanner capabilities and sensitivities, studies have demonstrated optimal tracer particle activity in practice where for low activity the rate of event detection is insufficient to measure a continuous trajectory and dynamic information is lost. Conversely, with activity too high, effects of pulse pileup and acquisition deadtime degrade the measurement, therefore for most applications 300 to 1000 μCi is required.

Objectives of the study

The primary objectives of this research are the following:

- Develop a standardised ^{18}F radiolabelling method using ^{18}F-FDG for PEPT Cape Town where results are reproducible and well characterised;
- Establish whether separation of ^{18}F from the glucose-complex of ^{18}F-FDG is required for the reactive solution used for radiolabelling, and if so, to develop a novel separation technique;
- Adjust parameters where necessary in producing the reactive solution used for radiolabelling;
- Improve the radiolabelling technique by implementing pre-treatment of the reactive solution used for radiolabelling;
- Confirm the resins in chloride form do not provide efficient uptake in comparison to fluoride form; and
- Confirm radiopurity of the radiolabelled resins.

The success of this work will have a vast contribution in extending the applications of PEPT and thus furthering the fundamental understanding of granular, fluid and multiphase flows in dynamic systems. PEPT Cape Town stands to be an immediate beneficiary for any of this development work, with equal impact for the PIC at the University of Birmingham over longer timescales. Furthermore, this work will enable institutes without access to accelerator facilities but with access to standard medical isotopes/equipment to have a greater involvement within the PEPT community.

Chapter 3

Experimental Procedure

This chapter will cover the apparatus and technique used in the development of ^{18}F tracer particles via chemical sorption for PEPT. In order for efficient uptake of ^{18}F, the resins were first converted to fluoride form. The resins were radiolabelled using pure ^{18}F-FDG as provided, followed by developing a ^{18}F-FDG separation technique to separate the glucose-complex and ^{18}F. The established radiolabelling methods were then improved upon. Additionally this chapter describes how measurements were performed to model adsorption profiles for each resin used in this study and obtaining gamma spectra of the various samples for verifying radiopurity.

3.1 Radioisotope supply

Throughout this research a variable supply of around 10 - 40 mCi in 500 μL of the radiopharmaceutical ^{18}F-FDG was provided by NRF-iThemba LABS Nuclear Medicine Department. NRF-iThemba LABS houses an 11 MeV cyclotron, as shown in Fig. 3.1a, where free ^{18}F^{-} ions in water are produced by irradiation of ^{18}O enriched water by a proton beam via the reaction ^{18}O(p,n)^{18}F. The isotope is then transferred to an automated rapid production cell and is utilised to synthesise commercially available ^{18}F-FDG.

Although it is advantageous to use free ^{18}F^{-} in water directly and it being the more accessible alternative world-wide at accelerator-based research facilities, in the context of the radioisotopes and accelerated beams available through NRF-iThemba LABS these methods offer the best, perhaps only, mechanism to utilising ^{18}F-based radiotracers for PEPT in South Africa. Although ^{18}F^{-} in water was unable to be sourced directly, a procurable source of ^{18}F-FDG was used as the radioisotope source of ^{18}F. Furthermore, this work reduces the need for daily isotope production by a dedicated cyclotron beam and the need for specialist

(a) (b)

Fig. 3.1 (a) 11 MeV Cyclotron used for producing ^{18}F and (b) representations of two rows of hot cells used for the chemical processing of radioisotopes [34].

equipment. Provided a suitable source of medical ^{18}F-FDG can be sourced, PEPT is therefore possible without the site constraints of an accelerator facility, enabling wider applications of the technique.

3.2 Chemical reagents and apparatus

All chemicals used were of analytical grade and purchased from Sigma Aldrich - Merck. These were: crystalline potassium fluoride (KF) ACS reagent $\geq$ 99.0%, methanol (CH_3OH) ACS reagent $\geq$ 99.8%, trifluoroacetic acid (TFA) ReagentPlus 99% and de-ionised water with conductivity greater than 18 MΩcm^{-1} obtained from a Millipore MilliQ Reagent Grade Water System. Gilson Pipetman P200N and P1000N were used in preparations for all solutions. The strong-base anion exchange resins Purolite A200 and A870 used in this study as the exchangers in uptaking ^{18}F and the radioactive tracers directly were kindly donated by Purolite South Africa.

In order to measure radioactivity, a Capintec CRC-25R ionisation chamber was used throughout all experiments using the in-built ^{18}F calibration.

3.3 Resin pre-treatment

The resins were pre-treated by adding 1M KF (100 mL, 100 mmol) to 5 g of untreated resin. After stirring for 10 min, the precipitate was allowed to settle and the supernatant removed and passed through a 2 mL syringe column with a 70 μm pore size.

The resins were rinsed with 10 mL of de-ionised water (10 times) and dried in a laminar fume hood for 48 - 72 hours. The treated resins were then transferred in a clean 250 mL wide-neck bottles and ready to be used for screening or selection for radiolabelling.

3.4 Radiolabelling directly with ^{18}F-FDG

^{18}F-FDG (5 - 7 mCi in 350 μL) was added to each reaction vial with resins contained and then placed on a mechanical shaker at 500 rpm to encourage exchange kinetics of the resins with a 100 W light bulb placed overhead at 5 cm above the reaction vial for evaporation. The resins were labelled in triplicate with each trial presented performed once (and strategically planned with respect to temporary limitations experienced in obtaining ^{18}F-FDG) such that the experimental standard deviation of the mean details the uncertainty in the activity measurements. The reaction was terminated when no further condensate was seen on the walls of the vial. Once visually dry, the radioactivity incorporated into each individual bead was measured and corrected for decay in reporting of results. To ensure that the activity measured was bound to each bead and not co-precipitated, a filtering test was performed where a small volume of milliQ water was rinsed over the bead to eliminate residue. An alternative method of rubbing each labelled bead between filter paper to cause abrasion proved to be effective and was used for the remainder of the research.

3.5 Radiolabelling using separated ^{18}F-FDG

3.5.1 Column separation method

For the column separation method devised during this research, Waters Sep Pak Waters tC18 6cc Vac columns were utilised. The column was activated prior to separation by adding CH_3OH (2 x 2 mL) followed by milliQ water (3 x 1 mL), under vaccum filtration. The column was stored in a preservation solution and activation replaced this solution and flushed out impurities, if any, remaining on the column.

The ^{18}F-FDG-TFA solution was then added to the column followed by milliQ water (5 times, 100 μL), and ^{18}F-TFA complex eluted which was then used as the source of ^{18}F. The fractions were measured and the highest activity vial(s) was used for further experiments.

This reactive solution was utilised with the same radiolabelling method described in Section 3.4 followed.

3.5.2 Modified radiolabelling with separated ^{18}F from ^{18}F-FDG

In seeking to improve the radiolabelling efficiency method described in Section 3.5.1, an adaption to the method was established by reducing the volume of the reactive solution used before radiolabelling. The column separation procedure as described in Section 3.5.1 was first implemented.

Instead of conical vials used as the reaction vial, two 200 mL Teflon beakers were used as the reaction vessel. These beakers were preheated at 190 °C on a hot plate with some water prior to radiolabelling and ideal for controlled heat distribution of the reactive solution. The reactive solution was then added to each beaker and heated for 3 min and 6 min in two respective trials with a 5 °C temperature decrease implemented to avoid aggressive heating and combustion of the radioactive solution. To redissolve any salt residue, 100 μL de-ionised water was added in each beaker and heated for 1 - 2 min.

The resins were then added to their respective beakers and alternated with being placed on a tilted shaker (positioned for optimal concentration and to avoid wide surface spread) for 2 min with an overhead 100 W bulb placed 5 - 10 cm from the beakers and on the hot plate set at 180 °C. The radiolabelling was terminated when condensate was noted on the walls of the vial and the beads were evaporated to dryness. The beads were then extracted from the reaction vial and measured for their activities.

3.6 Absorption profile modelling

In order to model absorption profiles for the ion exchange resins, each resin was weighed (1.2 mg) in seven separate vials. With a baseline concentration, ratios of 0.00005 M, 0.0001 M, 0.00025 M, 0.0005 M, 0.001 M, 0.0025 M and 0.005 M of hydrofluoric acid (HF) i.e ratios of 1/10, 1/5, 1/2, 1 (baseline), 2, 5 and 10 were made. Each vial was made up to 3 ml with milliQ water and then placed on the mechanical shaker at 500 rpm. Lastly, the activities were measured after 30 min and then at 60 min. From each single set of data the measured activity load per 1.2 mg of resin at varying concentrations was determined.

3.7 Measuring gamma spectra using a high purity germanium (HPGe) detector to verify radiopurity

As confidence check on the activity measurements and absence of radioactive contaminants, gamma spectra measurements were obtained using a high purity germanium (HPGe) detector of: a 169 μCi/4 μL sample of the provided ^{18}F-FDG, a 135 μCi/25 μL sample of the separated ^{18}F-FDG solution consisting of ^{18}F-TFA complex, a radiolabelled A200 and A870 bead with activity of 59.8 μCi and 72.4 μCi respectively and the background in the counting room. All measurements were recorded for 300 seconds (live time) with the samples placed with an open slit at a distance of 1 m from the detector.

Chapter 4

Results and Discussion

In performing measurements to quantify the radioactive decay at some time, decay correction is necessary as a result of the nuclide decaying during the acquisition time and this relies on adjusting the decay factor [48]. For example, if tracers are added to the radioactive solution for radiolabelling, collected in separate vials for measurements at the same time and the activity of the tracers are measured at a later time, decay correction allows estimation of the activity at the time it would have been measured. In other words, the tracers measured for their activities after the radiolabelling process will have to be decay corrected to reflect the decay that occurred between the two relevant events.

Once a reference time, time zero, is carefully distinguished and the timestamps of relevant measurement events identified, the activities at later times based on the reference time are decay corrected using the decay correction factor. As shown in Eq. 1.4, the exponential decay is described by the first-order ordinary differential equation and can be rearranged to

$$\frac{dN}{N} = -\lambda dt, \tag{4.1}$$

where integrating both sides then provides

$$\ln\left(\frac{N}{N_0}\right) = \lambda t, \tag{4.2}$$

and exponentiating yields the functional form of

$$N(t) = N_0 e^{-\lambda t}. \tag{4.3}$$

Therefore, N_0 is to be calculated with respect to a reference where the decay factor is calculated using the time elapsed and decay constant and divided into the uncorrected measurement. In this research the ^{18}F tracer development was categorised into two events: the first being separating ^{18}F-FDG and preparing the radioactive solution for radiolabelling and the second being the radiolabelling process and activity measurements of the tracers. Both events were decay corrected and the importance of decay correcting should be noted in order to compare activity measurements accurately.

Throughout this research a comparison of the uptakes relative of each sample to the starting activity concentration of the reactive solution used was needed as well, in particular to compare equivalent results that had different initial conditions. This was difficult as the initial conditions may change the chemical processes involved later in the labelling and factors such as self-absorption in the samples and differing absorption between beads and solutions also impact the outcome of the results. However, a standardised radiolabelling efficiency formula is defined as follows

$$\text{radiolabelling efficiency } \% = \frac{\text{measured radioactivity uptake}}{\text{theoretical radioactivity uptake}}, \tag{4.4}$$

where the measured radioactivity uptake is the average of the radioactivity of tracer particles measured at a certain time after defined time zero (decay corrected back to zero) and the theoretical radioactivity uptake is the decay corrected total initial radioactivity of the reactive solution that ideally should be uptaked by one tracer particle in theory, therefore divided by the number of beads. In actuality the theoretical radioactivity uptake capacity will never be met.

With respect to PEPT, it is convenient to report specific activity values as masses and activities, therefore expected for typical tracer particles. The theoretical minimum mass of radioactive substance required to produce a standard 1 mCi tracer particle can be calculated. Maximum specific activities per 1 mCi tracer are 24.59 pg/mCi and 10.51 pg/mCi for ^{68}Ga and ^{18}F respectively, implying that ^{18}F-based tracers can be made relatively smaller while maintaining optimum activity for tracking [49].

The activity concentration of the ^{18}F-FDG supplied was variable throughout this research and depended on the production for each supply by the Nuclear Medicine Department at NRF-iThemba LABS, therefore each radiolabelling experiment had varying activity concentrations of the reactive solution. Each trial is defined as having a corresponding ^{18}F-FDG activity concentration with the relevant reactive solution divided between two reaction vessels, with each reaction vessel having equivalent or near equivalent activity concentrations. Consequently, the volume of the reactive solution used varied as well to meet this requirement to ensure absolute activity results are comparable between the resins in each trial. A summary of the activity concentrations and corresponding volumes of the reactive solutions are detailed in the Appendix.

Although shaking and heating parameters were kept consistent during radiolabelling procedures, the period required for the radiolabelling procedure will also differ given the volume of the reactive solution and indeterminable kinetics and factors of the exchange reaction, however the requirement of evaporating and shaking the resins until dryness was the baseline of analysing the radiolabelling time required in each trial. Each reaction vessel contained three resin beads of either Purolite A200 or A870, which was then radiolabelled in triplicate to reduce uncertainty of resin bead uniformity.

In developing a novel ^{18}F radiolabelling technique for PEPT via chemical sorption methods using Purolite A200 and A870 resins and ^{18}F-FDG, establishment of radiolabelling using ^{18}F-FDG as the reactive solution was first investigated to determine whether a column chromatography method was to be implemented to separate the glucose-complex of ^{18}F-FDG and ^{18}F. After developing the separation method, the effectiveness of using the resultant ^{18}F-TFA complex was compared as well as determining the ratio of TFA:^{18}F-FDG required in the loading solution prior to separating the glucose-complex and ^{18}F. Thereafter, the radiolabelling method was improved upon by treating the reactive solution prior to radiolabelling. Once the radiolabelling and separation methods were established, resins in chloride form were confirmed to be less effective in uptaking ^{18}F in comparison to resins in fluoride form. Lastly, an overview on the radiopurity of the reactive solution and radiolabelled resins was studied.

4.1 Radiolabelling directly with commercial ^{18}F-FDG

A primary component in producing PEPT tracers is the radioisotope source such that activity can uptaken by the tracer particles. It was uncertain whether using ^{18}F-FDG as the reactive solution will suffice for the anion exchange resins Purolite A200 and A870 or if the glucose-complex of ^{18}F-FDG competes. Here the resins were radiolabelled, as described in Section 3.4, using ^{18}F-FDG provided in order to establish whether separation of ^{18}F-FDG was required.

In trial A1.1 and A1.2 a ^{18}F-FDG supply of 34 mCi in 500 μL was provided such that each reaction vial in trial A1.1 and A1.2 was loaded with 10 mCi and 11 mCi each in 165 μL respectively with a radiolabelling time of 30 min. In trial A2.1 and A2.2 a ^{18}F-FDG supply of 19 mCi in 500 μL was provided such that each reaction vial trial in A2.1 and A2.2 was loaded with 5.7 mCi and 5.6 mCi each in 165 μL respectively with a radiolabelling time of 50 min. Lastly, in trial A3.1 and A3.2 a ^{18}F-FDG supply of 39 mCi in 500 μL was provided such that each reaction vial in trial A3.1 and A3.2 was each loaded with 6.7 mCi in 160 μL with a radiolabelling time of 40 min.

As shown in Table 4.1, trial A3.1 and A3.2 provided the highest radiolabelling efficiency for corresponding resins with the second highest activity concentration of ^{18}F-FDG making up the reactive solution out of the three trials. Trial A1.1 and A1.2 yielded the lowest radiolabelling efficiency for both resins, however conversely had the highest activity concentration of the reactive solution in each reaction vial and shortest radiolabelling time required. The evaporation was likely rapid in comparison to the other two trials resulting in loss of ^{18}F-FDG as precipitate on walls of the reaction vials or combustion of ^{18}F-FDG salt. Across all trials the A870 resins consistently yielded a higher activity uptake than the A200 resins.

Table 4.1 Activity per bead radiolabelled of the A200 and A870 resins using ^{18}F-FDG directly with no ^{18}F separation techniques implemented.

	trial	diameter range (μm)	activity (μCi)	radiolabelling efficiency %
A200	A1.1	440 - 470	84.04 $\pm$ 0.77	2.3
	A2.1	430 - 440	71.7 $\pm$ 3.6	3.6
	A3.1	450 - 480	172 $\pm$ 92	7.4
A870	A1.2	520 - 570	278 $\pm$ 23	7.4
	A2.2	430 - 440	196.5 $\pm$ 2.9	10
	A3.2	470 - 490	324 $\pm$ 45	14

Despite the sufficient activity uptake achieved per bead, upon inspection during the radiolabelling procedure the ^{18}F-FDG appeared to crystallise and had a yellow-tinted coating encasing the beads across all trials listed in Table 4.1. This posed an issue as it was evident the activity achieved was that of the ^{18}F-FDG salt surrounding the bead and not ^{18}F labelled onto the resins itself. Additionally any ^{18}F-FDG salt or residue that got physically removed off the resins produced no radiolabelling. The ion exchange process was not responsible for activity transfer and attachment of radioactive ions were not closely bound to the resin. This is unsuitable for PEPT as activity gets easily removed from the tracer in typical applications and contaminating apparatus. This was shown in trial A3.1 where although the reactive solution concentration was adequately spread across the area of the reaction vial during the radiolabelling procedure, one of the resin beads displayed almost no radiolabelling (approximately 10 μCi, close to baseline) where the ^{18}F-FDG salt did not encase the resin but instead dried down on the wall of the reaction vial. This is also reflected in the variability of the results, particularly for trial A3.1, A1.2 and A3.2. The activities varied dependently on the crystallisation and degree of ^{18}F-FDG salt encasing the resins, which unfortunately cannot be manually controlled. Here the results reflected that the resin was not labelled with ^{18}F despite the sufficient exposure to the reactive solution and no residue affecting the resin. In comparison, the resin bead that displayed the highest activity radiolabelled had more excess ^{18}F-FDG salt encased than the others and similarly the lowest activity achieved corresponded to less ^{18}F-FDG salt encased on the resin.

It is evident that radiolabelling using ^{18}F-FDG to produce ^{18}F tracers via chemical sorption does not suffice. This then motivated for a separation method of the ^{18}F-FDG glucose-complex to be developed as described in Section 3.5.1 and its efficacy tested as the reactive solution used for radiolabelling.

4.2 Radiolabelling using separated ^{18}F from ^{18}F-FDG

Based on the ^{18}F radiolabelling outcome analysed using ^{18}F-FDG, a separation method of the ^{18}F-FDG glucose-complex was developed as described in Section 3.5.1.

Elution refers to the chromatographic technique of extracting an adsorbed substance from a adsorbing media using a solvent. The loading solution that needs to be separated along with the mobile phase (acts as an eluting agent) is introduced in the column and individual components are eluted out at different rates based on their adsorption and affinity to the adsorping media. The fraction of the mobile phase that acts as the carrier of the sample components is known as eluent and the mixture of solute and solvent that exits the column is known as an eluate [50].

In order to establish a novel column separation technique of the glucose-complex in ^{18}F-FDG and ^{18}F and improve separation of ^{18}F, the relative abundance of fluorine may need to be considered; TFA is a structural analogue of acetic acid with all three of the acetyl groups hydrogen atoms replaced by fluorine atoms. Therefore, if the TFA ratio in the loading solution is increased then the three fluorine atoms will compete with ^{18}F-FDG. In theory if ^{18}F has an activity of 40 mCi (1480 MBq) then relating the activity, A, to the number of moles via

$$A = \lambda N, \tag{4.5}$$

where N is the number of radioactive nuclei, indicates that there are 4.1×10^{-14} g or 2.3×10^{-15} moles of ^{18}F in 40 mCi and thus 7.6×10^{-16} moles of TFA for a 1:1 ratio. This indicates that the minimum volume of TFA required is 5.9×10^{-17} dm^3 to limit competing effects. It would not be possible to physically measure this borderline volume, however competing effects by varying the TFA ratio in preparing the loading solution were investigated.

As described in Section 3.5.1, a fixed volume (50, 100, 200, 500 or 1000 μL) of TFA was added to the 500 μL ^{18}F-FDG mixture and mechanically shaken for 1 - 2 min. This combined mixture was then decanted into the activated column and eluted with 500 μL of milliQ water.

The column has ^{18}F, TFA and FDG in milliQ water. The column absorbs the FDG and when eluted the ^{18}F is knocked off the column such that ^{18}F-TFA complex is produced as illustrated in Fig. 4.1. The column is then further eluted with 500 μL milliQ water such that an elution profile was developed and fractions collected in aliquots to use the ^{18}F-TFA complex as the reactive solution for radiolabelling resins Purolite A200 and A870. It is important to note that the ^{18}F-TFA complex likely contains a mixture of radioactive and non-radioactive fluoride. An overview of various TFA ratios used (volumes of 50, 100, 200, 500 or 1000 μL) in the loading solution is presented below. Note that elution profiles were developed across all experiments in this research, however for convenience only the elution profile for trial D1.1, D1.2, D2.1, D2.2, D3.1 and D3.1 (shown in Fig. 4.2) will be presented. The elution profile provides insight and development of the activity concentration of the ^{18}F-TFA complex used for radiolabelling. Although the activity concentration eluted is not capable of being controlled by an experimentalist, the captured eluates can be strategically used to make up a near desired reactive solution (with respect to activity concentration characteristics) for radiolabelling.

For the first experiment in separating ^{18}F from the glucose-complex, the loading solution of 50 μL TFA with 21 mCi ^{18}F-FDG in 500 μL (volume ratio of 1:10 of TFA:^{18}F-FDG) was prepared for trial B1.1 and B1.2 and 27 mCi ^{18}F-FDG in 500 μL was prepared for the remaining trials as shown in Table 4.2. The glucose-complex of ^{18}F-FDG was separated and ^{18}F eluted such that 17 mCi of ^{18}F-TFA complex was made up of the two highest activity eluates in trial B1.1 and B1.2 to prepare the reaction vial of trial B1.1 and B1.2 with 4.5 mCi/280 μL each. Similarly 25 mCi was made up of the three highest activity eluates to

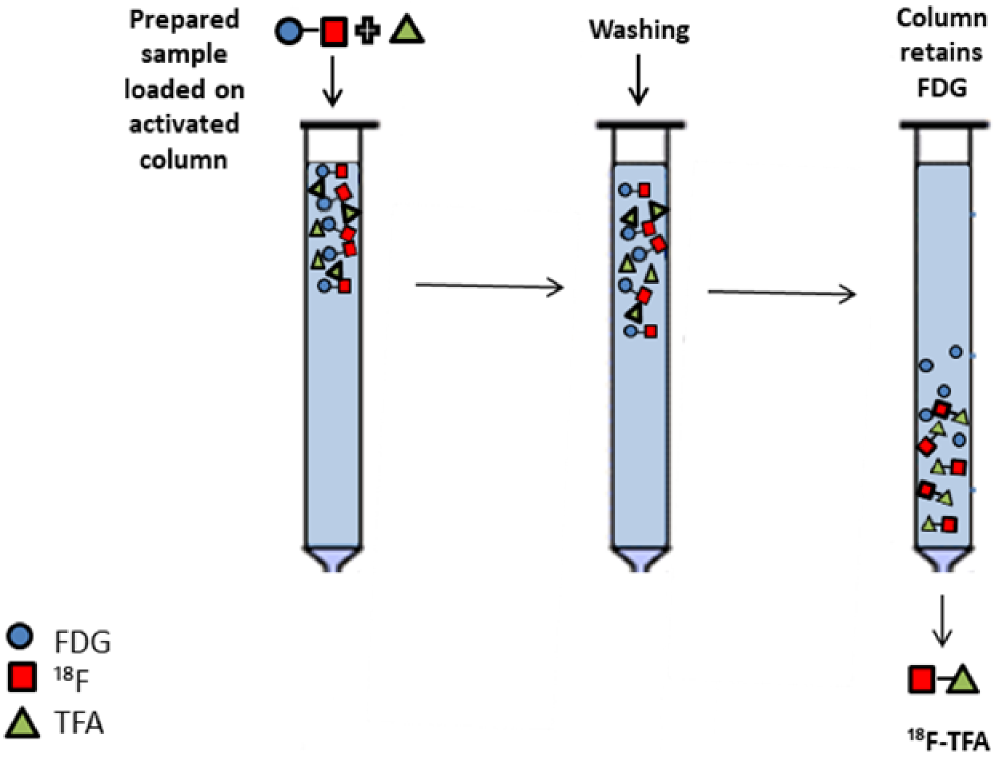

Fig. 4.1 Column separation procedure where the prepared ^{18}F-FDG and TFA solution is loaded on an activated Sep-Pak C18 column and eluted with milliQ water such that FDG is adsorbed.

prepare the reaction vial in trial B2.1 and B3.1 with 6.1 mCi/270 μL each and trial B2.2 and B3.2 with 5.0 mCi/270 μL each.

Similarly to the radiolabelling method described in Section 3.4, in preparation for the radiolabelling three beads were selected, placed in a reaction vial and this reaction vial was gently pre-heated prior to radiolabelling. Varying the resin size allows a greater insight to uptake differences. The ^{18}F-TFA complex solution as described above was then added to each reaction vial and placed in the holders on the mechanical shaker. A 100 W light bulb was placed overhead to provide heating for evaporation at a distance of 5 - 10 cm and the shaker was set at approximately 500 rpm. Every 12 - 15 min a check for overheating, and where necessary rotation, to ensure equivalent heat exposure for all vials was implemented. The radiolabelling was terminated once no liquid could be seen condensing on the walls of the vial and beads were evaporated to dryness. The beads were then extracted from the reaction vial and measured for their activities as shown in Table 4.2.

Table 4.2 Activity per bead radiolabelled using a TFA:^{18}F-FDG ratio of 1:10 prepared for the column separation.

	trial	diameter range (μm)	activity (μCi)	radiolabelling efficiency %
A200	B1.1	540 - 560	78.7 ± 6.6	5.2
	B2.1	560 - 580	71.7 ± 3.6	1.4
	B3.1	560 - 580	172 ± 92	2.9
A870	B1.2	530 - 580	104 ± 20	6.9
	B2.2	560 - 580	54.4 ± 7.1	3.3
	B3.2	560 - 580	31.7 ± 3.4	1.9

Across all trials in using a TFA:^{18}F-FDG ratio of 1:10 in the prepared loading solution, a hardened residue encased all beads in the reaction vial. Despite manually removing as much of the residue as possible, the chemical changes as a result of the evaporation applied in the radiolabelling procedure may cause combustion or crystallisation of the TFA salt in the span of the radiolabelling time and possibly lead to a loss of ^{18}F radiolabelling.

Although trial B2.1, B2.2, B3.1 and B3.2 had the higher activity concentrations in each reaction vial, trial B1.1 and B1.2 yielded the highest radiolabelling efficiency, as shown in Table 4.2, with A870 resins consistently showing greater uptake than A200 resins. There appeared to be great variance in trial B3.1 and B1.2 and no uptake trends can be established, therefore observing the visible chemical changes when varying the TFA ratio in the loading solution was priority in the following trials, despite the minimum TFA volume motivation.

In order to investigate the visible TFA salt residue and competitive effects, the TFA ratio in preparing the loading solution was increased to 100 μL TFA with 10 mCi (provided for trial C1.1 and C1.2), 17 mCi (provided for trial C2.1 and C2.2) and 18 mCi (provided for trial C3.1 and C3.2) ^{18}F-FDG in 500 μL such that the volume ratio is 1:5 of TFA:^{18}F-FDG. The column was eluted such that the ^{18}F-TFA separated solution of 9.1 mCi was made up of the two highest activity eluates in trial C1.1 and C1.2 to prepare the corresponding reaction vials with 3.3 mCi/350 μL each. Similarly 10 mCi was made up of the highest activity eluate in trial C2.1 and C2.2 to prepare the corresponding reaction vials with 5.0 mCi/225 μL each and 14 mCi was made up of the two highest activity elutes in trial C3.1 and C3.2 to prepare the reaction vials with 4.9 mCi/280 μL and 4.4 mCi/280 μL respectively.

Increasing the TFA ratio to 100 μL showed less excess TFA salt during and after the radiolabelling compared to the 1:10 loading solution trials. Additionally the salt was not as solidified and some residue attached loosely to the walls of the reaction vial. As shown

Table 4.3 Activity per bead radiolabelled using a TFA:^{18}F-FDG ratio of 1:5 prepared for the column separation.

	trial	diameter range (μm)	activity (μCi)	radiolabelling efficiency %
A200	C1.1	550 - 570	14.2 ± 2.6	1.3
	C2.1	530 - 590	19.5 ± 2.8	1.2
	C3.1	550 - 570	36.9 ± 1.6	2.2
A870	C1.2	540 - 570	16.4 ± 2.9	1.5
	C2.2	560 - 580	38.0 ± 2.4	2.4
	C3.2	540 - 570	58.6 ± 9.4	4.0

in Table 4.3, trial C1.1 and C1.2 had the lowest activity concentration in the reaction vials corresponding to the lowest radiolabelling efficiency and trial C3.1 and C3.2 produced the highest radiollabeling efficiency with the second highest activity concentration in the reaction vials. There was no significant relation between the activity concentration of the reactive solution and radiolabelling efficiency, however these results indicated that the excess TFA may result in loss of uptake with the reactive solution comprising of ^{18}F-TFA complex.

In the 200 μL trial (volume ratio 1:2.5 of TFA:^{18}F-FDG), 14 mCi (trial D1.1 and D1.2), 25 mCi (trial D2.1 and D2.2) and 18 mCi (trial D3.1 and D3.2) of 500 μL ^{18}F-FDG was provided. The highest activity eluants, shown in Fig. 4.2, were chosen to prepare the reaction vials containing A200 resins with 3.2 mCi/290 μL, 6.4 mCi/220 μL and 5.1 mCi/270 μL in trial D1.1, D2.1 and D3.1 respectively, as well as the reaction vials containing A870 reins with 3.2 mCi/290 μL, 6.5 mCi/220 μL and 5.0 mCi/270 μL in trial D1.2, D2.2 and D3.2 respectively. The activities achieved are shown in Table 4.4.

Table 4.4 Activity per bead radiolabelled using a TFA:^{18}F-FDG ratio of 1:2.5 prepared for the column separation.

	trial	diameter range (μm)	activity (μCi)	radiolabelling efficiency %
A200	D1.1	450 - 480	43.8 ± 5.1	4.1
	D2.1	550 - 590	78.2 ± 9.4	3.6
	D3.1	550 - 580	47.6 ± 6.9	2.8
A870	D1.2	430 - 480	91 ± 17	8.5
	D2.2	530 - 590	74 ± 15	3.4
	D3.2	570 - 590	30.8 ± 7.9	1.8

The 200 μL trials showed the highest radiolabelling efficiencies for both resins and displayed little to no salt residue during nor after the radiolabelling procedure. The 1:2.5

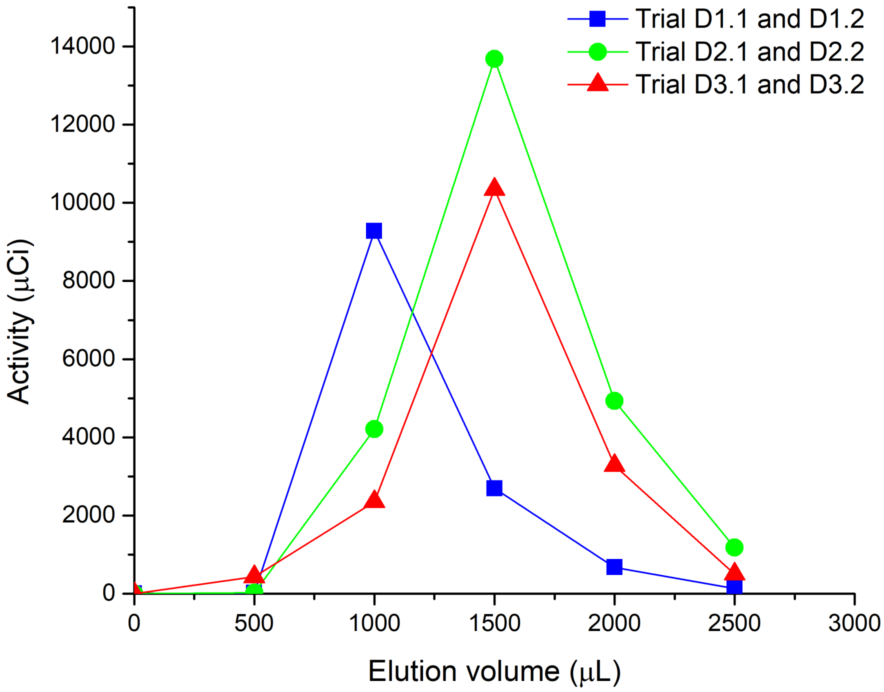

Fig. 4.2 Elution profile of separated glucose-complex with TFA:^{18}F-FDG ratio of 1:2.5 prepared as the loading solution such that fractions of ^{18}F-TFA complex are collected in aliquots to use as the reactive solution for radiolabelling resins Purolite A200 and A870.

loading solution produced the most consistent radiolabelling throughout all experiments with both A200 and A870 resins having adequate uptake.

The loading solutions of ratio 1:1 and 2:1 of TFA:^{18}F-FDG was also investigated to observe and confirm that excess TFA was not required in the loading solution. In the 500 μL TFA (volume ratio 1:1 of TFA:^{18}F-FDG) trials ^{18}F-FDG in 500 μL of 14 mCi was provided for E1.1 and E1.2, 15 mCi was provided for trial E2.1 and E2.2 and 29 mCi was provided for trial E3.1 and E3.2 The column separation extracted ^{18}F-TFA complex of 13 mCi from the highest activity eluate for trial E1.1 and E1.2, 10 mCi from the two highest eluates for trial E2.1 and E2.2 and 18 mCi from the highest activity eluate for trail E3.1 and E3.2. The reaction vials were prepared with 6.9 mCi/280 μL, 4.8 mCi/460 μL and 6.7 mCi/270 μL in trial E1.1,E2.1 and E3.1 respectively. Similarly the reaction vials were prepared with 6.7 mCi/275 μL, 5.1 mCi/460 μL and 6.8 mCi/270 μL in trial E1.2, E2.2 and E3.2 respectively.

For the 1000 μL TFA trial (volume ratio 1:0.5 of TFA:^{18}F-FDG), 17 mCi for trial F1.1 and F1.2, 22 mCi for trial F2.1 and F2.2 and 25 mCi for trial F3.1 and F3.2 of 500 μL ^{18}F-FDG was utilised. The separation yielded 7.2 mCi for trial F1.1 and F1.2, 9.5 mCi for trial F2.1 and F2.2 and 17 mCi for F3.1 and F3.2 of the ^{18}F-TFA complex from the highest activity eluates. The reaction vials containing A200 resins were prepared with 3.5 mCi/510 μL, 4.7 mCi/250 μL and 6.0 mCi/250 μL in trial F1.1, F2.1 and F3.1 respectively. Similarly the reaction vials containing A870 resins were prepared with 3.6 mCi/510 μL, 4.8 mCi/250 μL and 5.6 mCi/250 μL in trial F1.2, F2.2 and F3.2 respectively.

Both the 500 μL and 1000 μL TFA ratio trials displayed little excess TFA salt in the reaction vial nor encased on the resin beads, similar to the outcome in the 200 μL TFA trials. As shown in Table 4.6, trial F3.1 and F3.2 in the 1000 μL displayed the lowest radiolabeling efficiencies out of all trials across the loading solution ratio experiments. Although the activities obtained shown in Table 4.5 were sufficient as well, the radiolabelling efficiencies for both the 1:1 and 2:1 loading solution trials were lower than compared to the 1:2.5 trials. The results elude to that when the loading solution has a greater than 1:1 ratio of TFA:^{18}F-FDG the relative abundance effects of the fluorine in TFA outweighs the physical and chemical change effects in the radiolabelling.

Table 4.5 Activity per bead radiolabelled using a TFA:^{18}F-FDG ratio of 1:1 prepared for the column separation.

	trial	diameter range (μm)	activity (μCi)	radiolabelling efficiency %
A200	E1.1	410 - 430	29.3 ± 6.1	1.3
	E2.1	570 - 580	51.87 ± 0.72	3.2
	E3.1	540 - 560	60.7 ± 1.9	2.7
A870	E1.2	430 - 480	56 ± 14	2.5
	E2.2	570 - 580	68.3 ± 3.1	4.0
	E3.2	540 - 560	73.6 ± 1.8	3.2

As shown in Table 4.7 there was no correlation between the TFA ratio used in preparing the loading solution and the radiolabelling efficiency, however the A870 resins showcase a higher uptake than the A200 resins. Although the A200 has a higher total volume capacity, this expresses the number of active groups and this total capacity is never reached, whereas A870 offers the higher operating capacity thus greater reactive sites. It should be noted that the individual resin bead uptake will differ based on size (larger resin beads will offer

Table 4.6 Activity per bead radiolabelled using a TFA:^{18}F-FDG ratio of 1:0.5 prepared for the column separation.

	trial	diameter range (μm)	activity (μCi)	radiolabelling efficiency %
A200	F1.1	420 - 440	44.4 ± 5.4	3.8
	F2.1	510 - 550	56.2 ± 2.0	3.6
	F3.1	550 - 570	14.1 ± 1.9	0.70
A870	F1.2	450 - 490	35.8 ± 1.3	3.0
	F2.2	540 - 560	63.5 ± 2.1	4.0
	F3.2	550 - 570	19.38 ± 0.94	1.0

more exchange sites and thus likely achieve higher uptake), however the difference in ideally using pure ^{18}F in water will greatly differ from the novel separation method developed which yields ^{18}F-TFA complex as the reactive solution. The chemical changes in the reactive solution cannot be undisputed nor overlooked when considering the success of radiolabelling efficiency, thus making it difficult to conclude a direct relationship between the activity concentration of the reactive solution and the radiolabelling efficiency. Nevertheless, using separated ^{18}F from the glucose-complex proved to be reflective of effective radiolabelling and motivation provided in using 200 μL of TFA in the loading solution as it yielded the highest average activities and radiolabelling efficiencies for both the A200 and A870 resins, providing the optimal conditions for the radiofluorination.

Table 4.7 Average radiolabelling efficiencies and radiolabelling period of A200 and A870 resins using various loading solutions of TFA:^{18}F-FDG.

TFA:^{18}F-FDG	Average radiolabelling efficiency %		Average radiolabelling time (min)	
	A200	A870	A200	A870
1:10	3.2 ± 1.1	4.0 ± 1.5	37.7 ± 6.3	42.0 ± 7.0
1:5	1.57 ± 0.34	2.63 ± 0.74	76 ± 59	74 ± 61
1:2.5	3.52 ± 0.38	5.0 ± 2.0	55.0 ± 5.0	51.7 ± 7.6
1:1	2.41 ± 0.59	3.24 ± 0.42	33 ± 11	33 ± 11
1:0.5	2.7 ± 1.0	2.68 ± 0.87	49.0 ± 3.0	49.0 ± 3.0

There were no discernable trends shown in altering the TFA ratio in the loading solution and the radiolabelling time required, however there was an inconsistency in one of the 1:5 ratio trials with a great increase in radiolabelling time required; this was likely due to the additional remnants of the TFA salt that may have slowed down the evaporation of the liquid reactive solution below in the reaction vial during the radiolabelling process. The adverse effect of having the radiolabeling procedure too long in duration is loss in activity due to decay, thus limiting the specific activity.

Additionally in one of the 1:1 ratio trials an outlier arised with a decrease in radiolabelling time required; here the rate of evaporation may have been too fast, evident by the browning precipitate on the walls and edge of the reaction vial which may result in a decrease in radiolabelling efficiency due to the resin beads having less exposure to the reactive solution. This particular trial had the highest activity concentration in each reaction vial, however did not exhibit the highest radiolabelling efficiency. Similarly with the anomaly in the 1:5 ratio trial that required a higher radiolabelling time, although this trial had the highest activity concentration in each reaction vial, it did not produce the highest radiolabelling efficiency out of the three trials. This confirmed the need to have controlled heating, shaking and evaporation during the radiolabelling procedure that is not aggressive nor too gradual to encourage efficient uptake.

Despite the significant improvement of developing a separation technique to separate ^{18}F from ^{18}F-FDG and using the resultant ^{18}F-TFA complex as the reactive solution to successfully radiolabel A200 and A870 resins with fixed exchange of the radioactive ions, the aim was to achieve consistent radiolabelling of 200 - 300 μCi which unfortunately was still not met. This lead to motivation to treating the separated reactive solution of ^{18}F-TFA complex by reducing the volume prior to radiolabelling the A200 and A870 resins. The same column separation method was implemented as described in Section 3.5.1 with the loading solution prepared as a 1:2.5 of TFA:^{18}F-FDG throughout the experiments.

4.2.1 Improving ^{18}F uptake

Given that the loading solution prepared for the separation of ^{18}F and ^{18}F-FDG was optimal at a ratio of 1:2.5 of TFA:^{18}F-FDG, this was implemented for the duration of the research, however reducing the reactive solution volume may assist in reducing the radiolabelling time required, thus limiting the loss of ^{18}F due to decay. However, it was uncertain whether pre-treating the reactive solution, comprising of ^{18}F-TFA complex, by heating will compromise the succeeding radiolabelling of the A200 and A870 resins.

As a standard, approximately half of the volume of the reactive solution in each reaction vessel was reduced. This required 6 min alternating between heating at 190 °C and shaking at 1000 rpm. A 100 μL of milliQ water was then added to the reaction vessel to redissolve the remainder salt and evaporate for 1 – 2 min. Thereafter, the resin beads were added to the reaction vessel for uptake.

There was concern that the initial duration of heating the reactive solution may have been too long and resulted in combustion as pre-trial yields were rather low for the A200 resins due to over drying beyond the evaporation (as evident by browning in the beaker). This led to implementing temperature control where the reactive solution in each reaction vessel was heated at 190 °C and every 2 min decreased by 5 °C and instead the shaker was decreased to 500 rpm. Thereafter the same procedure followed in radiolabelling the resin beads as described in Section 3.5.1 and no combustion in either reaction vessel was observed. It is of importance to ensure the liquid reactive solution is concentrated and not spread out in the area of the reaction vessel as this limits the resin bead contact for uptake. This was overcome by tilting the shaker to ensure the beads were sufficiently submerged and in full contact with the reactive solution until dryness.

A provided supply of 19 mCi for trial G1.1 and G1.2, 16 mCi for trial G2.1 and G2.2 and 25 mCi for trial G3.1 and G3.2 of ^{18}F-FDG in 500 μL was used. The second and third highest eluates were used to make up the separated solution of 14 mCi for trial G1.1 and G1.2, 13 mCi for G2.1 and G2.2 and 20 mCi for G3.1 and G3.2. For the A200 reaction vessels, the activity concentration loaded for trial G1.1, G2.1 and G3.1 was 7.4 mCi/450 μL, 6.2 mCi/500 μL and 11 mCi/450 μL respectively. Similarly the A870 reaction vessels were loaded with 6.9 mCi/450 μL, 6.7 mCi/500 μL and 10 mCi/420 μL for trial G1.2, G2.2 and G3.2 respectively.

As shown in Table 4.8, the average activity radiolabelled per bead and radiolabelling efficiencies increased in comparison to the first radiolabelling method without altering the reactive solution. Trial G3.1 and G3.2 had the highest activity concentration of the reactive solution and displayed the highest average activity labelled as well as shortest radiolabelling time required on both the A200 and A870 resins. Although trial G1.1 and G1.2 had the second highest activity concentration, the A200 resins required a radiolabelling time deviating greatly compared to the other trials and showed slight damp salt. However, there was consistency in the radiolabelling efficiencies for trial G2.1, G2.2, G3.1 and G3.2. The A870 resins also consistently outperformed in uptake and radiolabelling efficiency, as expected due to having the higher operating capacity, with higher activity concentration of radioactive solution corresponding to higher activity radiolabelled per resin.

Table 4.8 Activity per bead radiolabelled using a TFA:^{18}F-FDG ratio of 1:2.5 prepared for the column separation in the adjusted radiolabelling method.

	trial	diameter range (μm)	activity (μCi)	radiolabelling efficiency %
A200	G1.1	570 - 590	80.5 ± 6.9	3.3
	G2.1	570 - 590	108.9 ± 3.6	5.2
	G3.1	550 - 590	183 ± 14	5.2
A870	G1.2	560 - 610	185 ± 15	8.1
	G2.2	550 - 590	174 ± 21	7.7
	G3.2	550 - 590	276 ± 16	8.1

It was established over the course of the above trials and pre-trials that evaporating the reactive solution longer than 6 min could likely evaporate almost all of the solution or cause adverse radiolabelling effects as a result of combustion. Therefore, this duration was investigated by heating the reactive solution for 3 min. A supply was provided with 20 mCi for trial H1.1 and H1.2, 22 mCi for trial H2.1 and H2.2 and 15 mCi for trial H3.1 and H3.2 of ^{18}F-FDG in 500 μL. The separation procedure yielded ^{18}F-TFA complex of 15 mCi for trial H1.1 and H1.2, 20 mCi for trial H2.1 and H2.2 and 11 mCi for trial H3.1 and H3.2 from the two highest eluates in each elution. The A200 reaction vessels were then loaded with 7.6 mCi/480 μL, 7.2 mCi/400 μL and 5.4 mCi/385 μL for trial H1.1, H2.1 and H3.1 respectively. The A870 reaction vessels were loaded with 7.6 mCi/480 μL, 6.5 mCi/400 μL and 5.5 mCi/385 μL for trial H1.2, H2.2 and H3.2 respectively.

As shown in Table 4.9, trial H2.1 and H2.2 yielded the highest activity uptake for both resins and had the highest activity concentration of the radioactive solution. Trial H3.1 and H3.2 had the lowest activity concentration of the reactive solution and lowest activity uptake and radiolabelling efficiency of its A200 bead. It is noted that the size variations in the resin beads likely reflect the uptake differences in these trials, however this was chosen to provide insight into the size effects although not modelled in this research.

It was observed the A870 resins continued to outperform in uptake and radiolabelling efficiency compared to the A200 resins. The second radiolabelling method presented proved to be superior in effectively radiolabelling the resin beads with a higher activity compared to the initial method where no evaporation treatment was done on the reactive solution prior to radiolabelling. The evaporation of the reactive solution may assist in reducing the excess TFA salt alone in solution and increasing the concentration; therefore there was less excess salt in reducing the separated solution for 6 min compared to 3 min.

Table 4.9 Activity per bead radiolabelled using a TFA:^{18}F-FDG ratio of 1:2.5 prepared for the column separation in the adjusted radiolabelling method.

	trial	diameter range (μm)	activity (μCi)	radiolabelling efficiency %
A200	H1.1	570 - 590	50.5 ± 6.0	2.0
	H2.1	540 - 600	91 ± 27	3.8
	H3.1	470 - 490	24.4 ± 1.2	1.3
A870	H1.2	570 - 590	60.8 ± 5.8	2.4
	H2.2	550 - 590	118 ± 18	5.4
	H3.2	470 - 490	76.1 ± 7.1	4.2

As a result, both the 3 min and 6 min trials consequently required a substantially lower radiolabelling time and processing compared to the initial method, thus limiting the loss of radioactivity due to decay. As shown in Table 4.10 there were variations in the radiolabelling times required and differed case to case, regardless of the reactive solution volume, but likely owes and adjusts according to the chemical changes throughout the processing of the reactive solution prior to radiolabelling and during radiolabelling once the beads are added to the reaction vessel.

Table 4.10 Average radiolabelling efficiencies and radiolabelling period of A200 and A870 resins using 1:2.5 loading solutions of TFA:^{18}F-FDG for durations of 3 min and 6 min of evaporating the reactive solution prior to radiolabelling.

	Period of evaporation (min)	Average radiolabelling efficiency %	Average radiolabelling time (min)
A200	6	4.6 ± 1.1	17.2 ± 9.5
	3	2.4 ± 1.2	4.7 ± 2.1
A870	6	7.98 ± 0.20	16 ± 10
	3	4.0 ± 1.5	3.67 ± 0.58

Confirmation of the requirement for the resins to be used in an ionic form with a lower selectivity for the functional group than the sample ions to be exchanged is needed to conclude the overall radiolabelling success presented in this research. In using the developed radiolabelling method described in Section 3.5.2 where the reactive solution of ^{18}F-TFA complex is evaporated for 6 min prior to radiolabelling, experiments radiolabelling both A200 and A870 resins in chloride form as provided was performed.

4.3 Validating efficient uptake in comparison to anion exchange resins in chloride form

As discussed in Section 2.2.2, strong-base anion exchange resins are less affected by water pH or hydroxide ions since the affinity of $^{18}F^-$ ions is stronger than hydroxide ions of resins and therefore suitable in utilising in producing ^{18}F tracers via chemical sorption techniques. The A200 and A870 resins are both quaternary ammonium derivatives in chloride form: $R\text{-}CH_2N(CH_3)_3^+Cl^-$, where chloride is the counter ion. However, because the affinity of the $^{18}F^-$ ion to the functional groups is much weaker than the Cl^- ion, the resin particles must first be converted into fluoride form e.g. $R\text{-}CH_2N(CH_3)_3^+F^-$, such that the converted F^- ions act as counter ions that exchange with $^{18}F^-$ ions. A confirmation of this was done by attempting to radiolabel the A200 and A870 resins in chloride form, which was provided in this form prior to pre-treatment detailed in Section 3.3.

A supply of 21 mCi for trial I1.1 and I1.2, 13 mCi for trial I2.1 and I2.2 and 17 mCi for trial I3.1 and I3.2 of ^{18}F-FDG in 500 μL was provided. The column separation procedure detailed in 3.5.1 was implemented where the two highest eluates were used to make up 15 mCi for trial I1.1 and I1.2 and 12 mCi for trial I3.1 and I3.2; the reaction vessels were loaded with 7.7 mCi/470 μL for trial I1.1 and 7.5 mCi/470 μL for trial I1.2 of the ^{18}F-TFA complex. Similarly reaction vessels were loaded with 5.8 mCi/370 μL for trial I3.1 and I3.2 respectively. For trial I2.1 and I2.2 the two highest eluates were selected as well as a volume of 150 μL from the third highest eluate to make up the corresponding vessels of ^{18}F-TFA complex with 5.3 mCi/500 μL and 5.1 mCi/500 μL respectively. Instead of using the A200 and A870 resins in the converted fluoride form, the resins in chloride form were used in the radiolabelling procedure as detailed in Section 3.5.2.

From the results shown in Table 4.11, the A200 and A870 resins had an average radiolabelling efficiency of (2.01 ± 0.55) % and (2.85 ± 0.43) % respectively. As expected, a decrease in the average activity radiolabelled per bead and the radiolabelling efficiencies across both resins is observed. There is minimal deviation from the three trials which confirms that strong-base anion exchange resins in fluoride form efficiently uptake ^{18}F in comparison to chloride form.

Therefore, in order for the ion exchange of the radioactive ions to occur, the radioactive ions must have a higher affinity for the resin than the counterions. The resin utilised should be used in an ionic form with a lower selectivity for the functional group than the sample

Table 4.11 Activity per bead radiolabelled using untreated resins.

	trial	diameter range (μm)	activity (μCi)	radiolabelling efficiency %
A200	I1.1	470 - 530	35.33 ± 0.88	1.4
	I2.1	450 - 480	40.4 ± 2.1	2.3
	I3.1	460 - 480	46.00 ± 0.12	2.4
A870	I1.2	470 - 500	58.7 ± 3.0	2.6
	I2.2	450 - 480	53.4 ± 2.1	3.1
	I3.2	460 - 500	59.2 ± 5.4	3.1

ions to be exchanged.

In Fig. 4.3 and Fig. 4.4 an overview of the absolute activity and efficiency for both the A200 and A870 resins is presented across each primary trial where each primary trial includes the three sets corresponding to each resin. For example, trial A for the A200 resins includes the results of A1.1, A2.1 and A3.1 and the uncertainty reflected by the standard deviation of these results, similarly for the remaining trials.

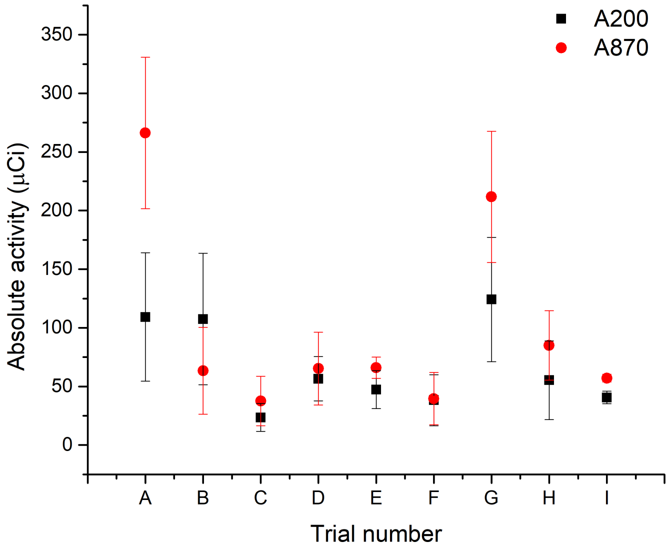

Fig. 4.3 An overview of the absolute activity for each primary trial for the A200 and A870 resins.

The variation in trial A validates that using ^{18}F-FDG as the reactive solution for radiolabelling A200 and A870 resins was that of the ^{18}F-FDG salt surrounding the bead and not ^{18}F labelled onto the resins itself, thus resulting in great variety in each trial. Additionally the

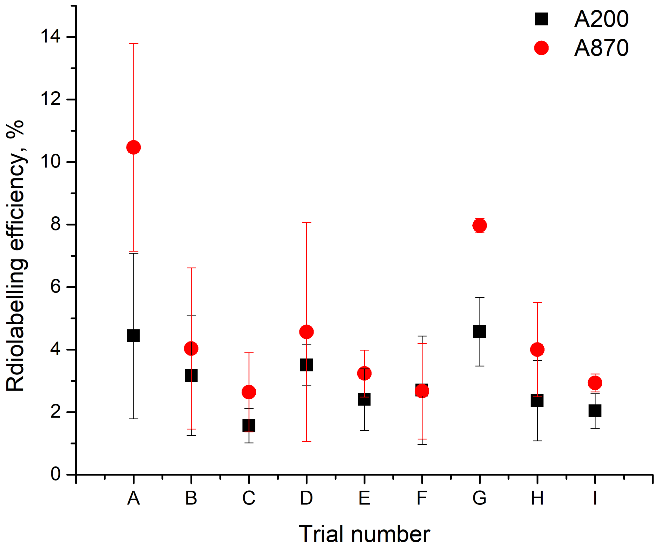

Fig. 4.4 An overview of the efficiency for each primary trial for the A200 and A870 resins.

A200 and A870 resins are not in experimental agreement. In summary, the average activity radiolabelled per resin and radiolabelling efficiencies increased in radiolabelling experiments G where the reactive solution was pre-treated prior to radiolabelling. Trial G yielded the highest absolute activity and efficiency, however the variation stems from the A200 resins, in particular requiring a radiolabelling time deviating greatly compared to the other trials, but there was consistency in the radiolabelling efficiency for the A870 resins. Overall the A870 resins also consistently outperformed in uptake and radiolabelling efficiency as expected.

In order to gain insight on the performance of the A200 and A870 resins, adsorption profiles can be modelled. Unfortunately this can be difficult to compare to [24] where ^{18}F is used, however using HF can be used as a means to model the concentration.

4.3.1 Adsorption profile modelling

To model the adsorption profiles of the A200 and A870 resins, the exchange is expected to be pronounced in the first few minutes of the radiolabelling, therefore 1 mL of the reactive solution was extracted and activity measured every minute for the first 10 min. The activity was then measured every 2 min for the next 10 min. Lastly, the activity was measured after 30 min and then at 60 min. The activity that should be loaded per 1.2 mg of resin at varying concentrations was determined. Unfortunately pure ^{18}F was not accessible, however HF was utilised, as described in Section 3.6, as a means to vary the concentration.

The bulk of the uptake during the radiolabelling procedure occurs within the first 20 min, therefore expansion in this region is shown in Fig. 4.5b and Fig. 4.6b for both the A200 and A870 resins respectively. Relating the capacity of the relevant resins A200 and A870, valence and atomic mass of ^{18}F, theoretically 23.4 g of F should be adsorbed by 1 kg of resin following the relation of

$$\text{mEq} = \frac{\text{mg}}{\text{atomic weight.valence}}, \tag{4.6}$$

and therefore 1.2 mg of the resin can adsorb 2.8×10^{-5} g of F. Relating this to the molar mass M ($n = m/M$), 1.6×10^{-6} mol of F can be uptaked by 1.2 mg of resin. A 3 mL solution of HF and de-ionised water (keeping in mind theoretically ^{18}F will be on a microlitre scale) such that the baseline concentration is 5×10^{-4} M and we explored these ranges further in ratios of 1/10, 1/5, 1/2, 2, 5 and 10 as well. The corresponding concentrations of HF was loaded in seven separate reaction vials with 1.2 mg of resin, and the remainder of the 3 mL was made up with milliQ water accordingly. The exchange was expected to be pronounced in the first 10 min of the radiolabelling, therefore a pipette was used to draw 1 mL of the solution and measured the activity in the ionisation chamber every minute for the first 10 min. Given that activity was measured for 1 mL/3 mL, the vial represents a third of all free ^{18}F in solution and anything not in solution is on the 1.2 mg of resin. Therefore, the activity of 1.2 mg of resin was determined by

$$\text{total activity in vial - 3(measured sample of 1 mL).} \tag{4.7}$$

This process was continued and the activity measured every 2 min for the next 10 min. Lastly, the activity after 30 min and then at 60 min was measured. From the data the activity that should be loaded per 1.2 mg of resin at varying concentrations was determined.

As shown in Fig. 4.5, the second highest concentration provided the highest uptake on 1.2 mg of A200 resin. An uptake peak across all trials within the first 10 min of the radiolabelling is observed until reaching a plateau and steadily decaying. Initially the uptake efficiency is high, due to the relative concentration of free ^{18}F^{-} ions within the solution and the availability of active exchange sites. As the reaction progresses, the concentration of free ions drops, exchange sites become populated, and the resulting free counter ion concentration increases. These effects serve to limit the progress of the exchange reaction, thus the activity obtained on the bead reaches a plateau based on the relative strength of each factor (e.g. number of active exchange sites, concentration of $^{18}F^{-}$ and counter ions, etc.). Over extended durations the bead activity is observed to decay, with a rate given by the radioactive decay of the ^{18}F isotope. It is not clear if any sites occupied by $^{18}F^{-}$ ions that undergo radioactive decay are freed following the decay and are able to recapture free ions from the solution, or if the resultant $^{18}O^{-}$ ion remains bound to the resin and prevent replacement uptake.

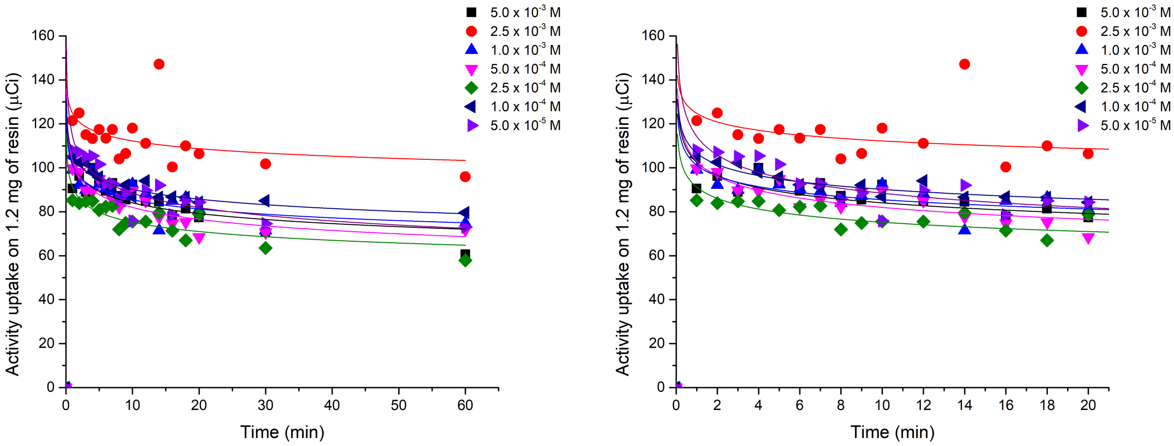

(a) (b)

Fig. 4.5 (a) Adsorption profile on 1.2 mg of A200 resin using varying HF concentrations and (b) detail of the first 20 min of the adsorption.

Similarly the three highest concentrations provided the highest uptake on 1.2 mg of A870 resins with an uptake peak occurring within the first 10 min of the radiolabelling, a maximum capacity reached and steady decay as shown in Fig. 4.6. Unexpectedly, in comparison to previous results and discussion, despite A870 resin having greater working capacity than the A200 resin, the A200 outperforms the A870 resins in uptake in these profile modelling experiments. Therefore, for further work on this study, a pure source of ^{18}F should be used for better insight into the kinetics.

It is still proven to be complex to experimentally model capacity as various factors such as the cross-linked resin used, the ion being exchanged, the counter ion in the solution and the temperature performed at has to be considered. However, from Fig. 4.5a and Fig. 4.6a an empirical resin capacity is evident over the long time scale of 60 min.

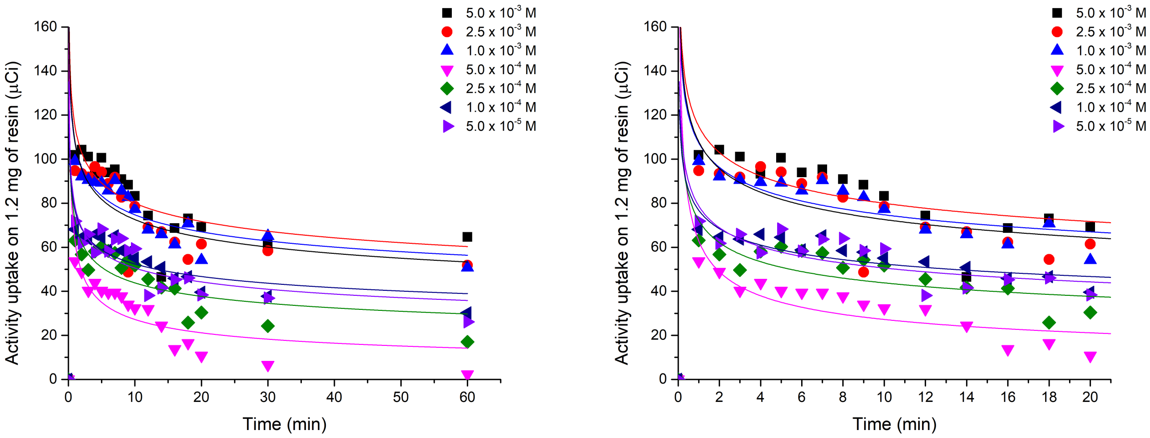

(a) (b)

Fig. 4.6 (a) Adsorption profile on 1.2 mg of A870 resin using varying HF concentrations and (b) detail of the first 20 min of the adsorption profile.

Throughout this research ionisation chambers, as used for measurements described in the Experimental Procedure, are of absolute activity and are only accurate if the sample is radioisotopically pure. Therefore, as a conclusion to successful radiolabelling and developing ^{18}F tracers, a purity confirmation using a spectrometer to validate ^{18}F uptake is required. The results are presented in Section 4.4.

4.4 Confirming radiopurity

Given that medical grade ^{18}F-FDG was used throughout this research, the radioisotope source itself is radioisotopically pure and exhibits no contaminants, therefore the activities measured should be that of ^{18}F and no other radiosiotopes. It is therefore appropriate to use ^{18}F calibration for ionisation chamber measurements.

To confirm radioisotopic purity, and as an independent verification for activity, a HPGe detector was used to measure gamma ray spectra of the reactive solution used for radiolabelling as well as the produced tracers. HPGe detectors are semiconductor detector crystals that are manufactured from ultrapure germanium and can be used to identify radioactive material. HPGe detectors have excellent energy resolution for gamma ray spectroscopy, meaning the detector can discriminate between gamma rays with similar energies. A sharp delta-function is ideal however what is reflected in the spectra is a peak structure usually Guassian in shape.

The width of this peak arises due to fluctuations of the statistics of ionisations and excitations. Therefore the resolution is given in relation of the full width at half maximum of the peak (FWHM), defined as the width of the distribution at a level that is just half the maximum ordinate of the peak, as R = FWHM/H_0 where H_0 is the peak centroid, illustrated in Fig. 4.7. A sodium iodide (NaI) detector typically has 8 - 9% resolution for gamma rays of the order of 511 keV whereas germanium detectors have resolutions on the order of 0.1%.

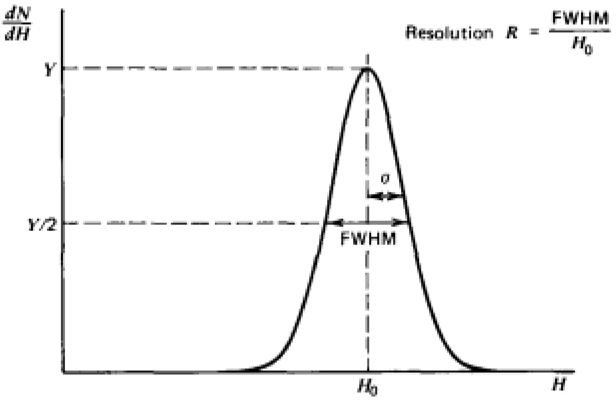

Fig. 4.7 Illustration of detector resolution where the peak with Gaussian shape has standard deviation σ and the FWHM defined as 2.35σ.

The gamma spectra of the ^{18}F-TFA complex reactive solution used for radiolabelling, radiolabelled A200 and A870 resins were recorded as described in Section 3.7 (with background activity subtracted and accounted for) to observe the 511 keV emission peak. Once measurements were taken, the energy calibration curve was determined by relating the relationship between the energy of a gamma photon and the centroid channel number of the peak produced by that gamma photon. The spectra summary sheet provided the peak analysis of known energies. As shown in Fig. 4.8 - 4.10, no contaminants are observed as pure ^{18}F-FDG was utilised throughout this research.

Any chemical processing, such as separating the ^{18}F-FDG complex to produce ^{18}F-TFA complex, will not change the radiopuriry. There was no record of external radioisotopes affecting the radiopurity of the reactive solution nor the radiolabelled resins. In Table 4.12, the measured photopeaks reflects those of the expected 511 keV photons. As described, ^{18}F decays dominantly (97%) via β^+-decay such that ^{18}F decays to ^{18}O releasing a neutrino and a positron. The electromagnetic radiation results from the positron-electron annihilation

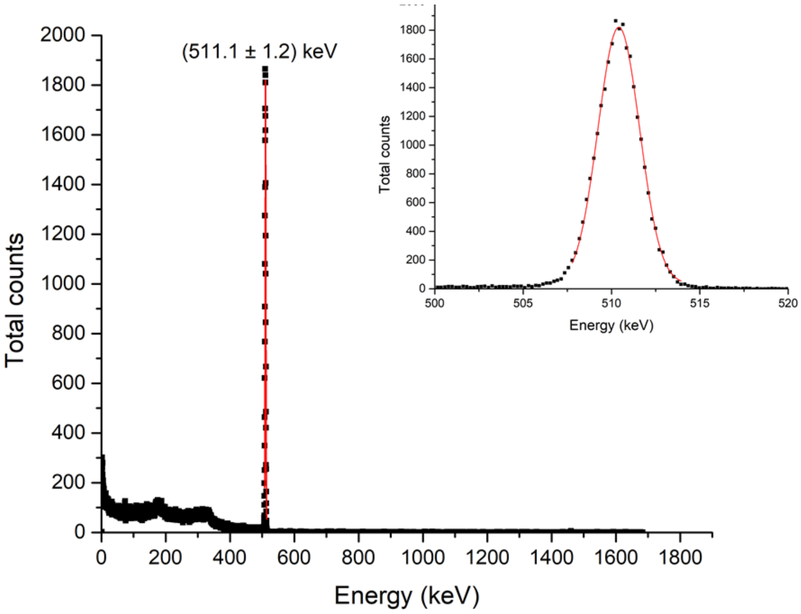

Fig. 4.8 Spectroscopy of the resultant ^{18}F-TFA complex used as the reactive solution for radiolabelling showcasing the full energy measurement with the inset showing detail in the 511 keV region. The reactive solution activity concentration measured was 135 μCi/25 μL and the spectra was recorded 2 hrs after elution.

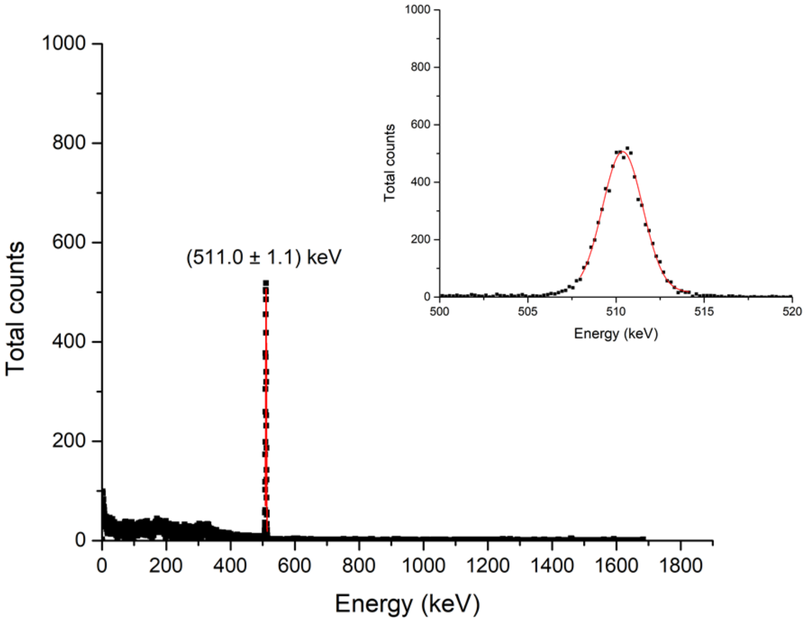

Fig. 4.9 Spectroscopy of a radiolabelled A870 resin showcasing the full energy measurement with the inset showing detail in the 511 keV region. The A200 resin was measured 2 hrs after radiolabelling procedure with an activity of 60 μCi.

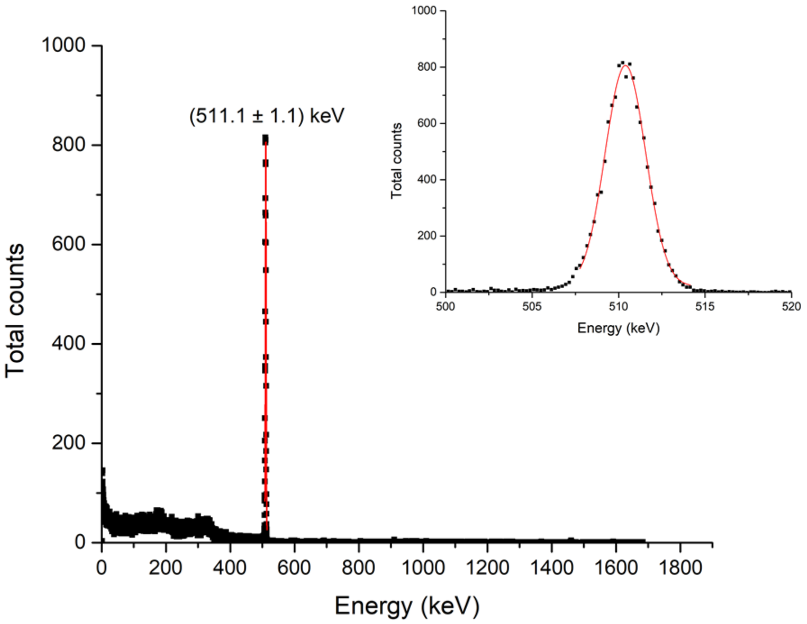

Fig. 4.10 Spectroscopy of a radiolabelled A870 resin showcasing the full energy measurement with the inset showing detail in the 511 keV region. The A8700 resin was measured 2 hrs after radiolabelling procedure with an activity of 72 μCi.

where two photons, each with energy 511 keV, are emitted.

Table 4.12 Photopeak analysis of the resultant ^{18}F-TFA complex after separating ^{18}F from the glucose-complex of ^{18}F-FDG and radiolabelled Purolite A200 and A870 resins.

	^{18}F-TFA complex	A200 resin	A870 resin
Measured photopeak (keV)	511.1	511.0	511.1
σ_x	1.2	1.1	1.1
FWHM	2.73	2.65	2.66
Resolution %	0.53	0.52	0.52

The HPGe spectroscopy results demonstrate a strong annihilation photopeak at 511 keV and associated continua as expected for a pure positron emitting source such as ^{18}F. Over the full energy scale measured there are no other statistically significant features, pointing towards high radio-purity samples. The figure insets show the region around the 511 keV annihilation photopeak in each case, where the areas of each peak are proportional to the absolute activity of the sample at the measured time. The proportionality constant is determined by the solid angle subtended by the source-detector system and the detector efficiency at 511 keV, and results are consistent with those measured with the ionisation chamber after correcting for decay. Acquisition deadtime potentially deviates from the proportional response, but the measured rates in these cases are low enough that these non-linear effects are negligible. The results give high confidence in the characterisation of the produced tracer particles in terms of isotopic content and activity. Although other radioactive contaminants are not expected, the glucose complex of ^{18}F-FDG will inevitably result in chemical contaminants and potential competing reactions that inhibit the tracer labelling abilities.

HPGe results are consistent with the ionisation chamber measurements within experimental uncertainty, thus justifying the use of the ^{18}F calibration for the ionisation chamber in all measurements. The gamma spectra of the relevant components measured concludes the success of developing ^{18}F based tracers for PEPT Cape Town using the chemical sorption techniques presented in this research. Despite ^{18}F-FDG being insufficient to use directly as the reactive solution for radiolabelling as a result of lack of the ^{18}F ions exchanged on the active sites of the A200 and A870 resins, a novel separation technique producing ^{18}F-TFA complex was successful in using as the reactive solution for radiolabelling and radiopurity confirmed any chemical processing done did not affect the radiopurity.

Chapter 5

Conclusion

PEPT has been extensively used in the study of flow particularly with experimental data allowing fundamental models to be developed and further optimised. It is crucial that the tracer materials used in PEPT are of sufficient radioactivity and near-identical to the bulk of the system in order for the PEPT data to be reflective of the motion in the system.

The primary objective of this study was to develop a ^{18}F tracer particle radiolabelling technique for PEPT Cape Town. If the materials in the system contain natural oxygen, are thermally stable and greater than 1 mm in diameter, tracer particles may be directly produced by activation in a suitable cyclotron beam as previously established. For routine work, and for tracer particles below 1 mm in diameter, PEPT Cape Town utilises chemical sorption methods to produce tracer particles. Unfortunately ion exchange resins are typically not representative of the particles of interest due to differences in density or surface chemistry properties; however, applying suitable coating layers to modify these properties improves representation. Advantageously, chemical methods can be employed to produce PEPT tracer particles of microscopic size. Therefore, great advantage lies in producing tracers via chemical sorption techniques, particularly in expanding the tracer development at PEPT Cape Town. At PEPT Cape Town, chemical sorption techniques based on ^{68}Ga has been well established and development of equivalent ^{18}F based methods where daily direct activation and/or free ^{18}F ions in water are not readily available was developed and impactful given the advantages of using ^{18}F based tracers in comparison to ^{68}Ga. The objective was to achieve consistent radiolabelling of 300 - 1000 μCi for anion exchange resins < 1 mm in diameter.

Commercially available medical grade ^{18}F-FDG was utilised as the ^{18}F radioactive source and initially as the reactive solution for radiolabelling Purolite A200 and A870 resins, however the activity achieved per resin was that of the ^{18}F-FDG salt surrounding the bead and not

^{18}F labelled onto the resins itself. A column chromatography method was then developed to separate the glucose-complex of ^{18}F-FDG in preparation of the reactive solution, comprising of ^{18}F-TFA complex, used for radiolabelling. The loading solution parameters were analysed and a 1:2.5 volume ratio of TFA:^{18}F-FDG proved to provide the greatest radiolabelling efficiency. Using the eluates obtained from the separation, reaction vessels were prepared having equivalent or near equivalent activity concentrations. Consequently, the volume of the reactive solution used varied as well to ensure absolute activity results are comparable between the resins in each trial. The highest activity achieved by the Purolite A200 and A870 resins was 80 μCi and 100 μCi over a range of 430 - 590 μm in diameter respectively.

Thereafter the radiolabelling method was improved upon by treating the reactive solution (^{18}F-TFA complex), resulting in a reduced reactive volume prior to radiolabelling. This reactive solution was heated for 6 min and 3 min and the A870 resins continued to outperform in uptake and radiolabelling efficiency compared to the A200 resins. This method developed proved to effectively radiolabel the resins with a higher activity of up to 200 μCi and 300 μCi over a range of 550 - 610 μm in diameter for A200 and A870 respectively compared to the initial method. Both the 3 min and 6 min trials consequently required a substantially lower processing time and limited the loss of radioactivity due to decay. Prior to radiolabelling the A200 and A870 resins were converted to fluoride form to provide efficient uptake, however radiolabelling resins in chloride form was also validated to show that in order for the ion exchange of the radioactive ions to occur, the radioactive ions must have a higher affinity for the resin than the counterions. The resin utilised should be used in an ionic form with a lower selectivity for the functional group than the sample ions to be exchanged. The gamma spectra of the measured radiolabelled A200 and A870 resins as well as the reactive solution concluded that the novel separation technique developed producing ^{18}F-TFA complex was successful in using as the reactive solution for radiolabelling. Chemical processing does not affect the radiopurity and the 511 keV emission peaks measured reflected the expected electromagnetic radiation resulting from the positron-electron annihilation.

These novel developments extend the application of PEPT at existing facilities and enables PEPT to be employed in applications without access to accelerators or dedicated hot-cell radiochemical laboratories.

Future work recommendations

The experimental limits using the developed radiolabelling method presented needs to be characterised in this case and competing ion exchange kinetic models, if any, identified. The chemical exchange and decaying concentration of radioactive species should be developed to determine the change in chemistry over time as the radioactive species decay to stability and as ions exchange with the introduced media. Once static chemical properties are quantified, additional factors such as agitation and heating can be realised.

As motivated in the research, ^{18}F is a pure β^+ emitter with no additional gamma emissions, therefore the signal to noise ratio in PEPT measurements is increased in comparison to ^{68}Ga. As ^{68}Ga is a β^+ emitter with higher energy, consequently the uncertainty of detection increases. Additionally the longer half-life of ^{18}F allows for extended experimental timescales. A detailed comparison between ^{18}F and ^{68}Ga tracers in both stationary and moving tracking using PEPT is also needed to confirm ^{68}Ga lower positron emission branching ratio and compare the location points and effects on tracking and location errors. confirmation of ^{68}Ga lower positron emission branching ratio, comparing location points of ^{18}F and ^{68}Ga and effects on tracking and location errors.

Although significant developments have been made in developing ^{18}F tracers for PEPT using ^{18}F-FDG, additional investigation producing ^{18}F in aqueous solution would be beneficial. This research was limited in obtaining ^{18}F in aqueous solution, but is typically produced and accessible at other accelerator-based facilities and is a financially viable and reliable source of ^{18}F. Development of tracer particle production based on the ^{16}O(α,pn)^{18}F nuclear reaction can be extended where the proposed alpha particle reaction a natural water target can produce ^{18}F in aqueous solution. This technique can be explored to maximise production and model total activation yield with experimental parameters. However, there are risks of side reactions occurring resulting in undesired radionuclides produced in the activation and compromising the high purity of ^{18}F. This novel method will complement the newly developed radiochemical method using ^{18}F-FDG presented in this research in reproducibility with respect to standardising and characterising ^{18}F radiolabelling methods.

References

[1] J. Clayden, N. Greeves, and S. Warren, Organic Chemistry, 2nd Edition, Oxford University Press, London, 2012.
[2] Cyclotron Produced Radionuclides: Principles and Practice, *Technical Reports Series n.o 465*, International Atomic Energy Agency (IAEA), Vienna, 2008.
[3] R.J. Blin-Stoyle, Nuclear and Particle Physics, Chapman Hall, London, 1991.
[4] G.F. Knoll, Radiation Detection and Measurement, John Wiley Sons Inc, New York, 1979.
[5] J.V. Jelly, Cerenkov Radiation and its Applications, Pergamon Press, London, 1958.
[6] D.B. Cassidy and A.P. Mills Jr, The production of molecular positronium, *Nature*, **449**, 195 - 197, 2007.
[7] A. Morrison, Using positron emission particle tracking (PEPT) to investigate the motion of granular media in a laboratory-scale tumbling mill, Master's Thesis, University of Cape Town, 2012.
[8] S.G. Karshenboim, (2003), Precision Study of Positronium: Testing Bound State QED Theory, *International Journal of Modern Physics A*, **19**, 879 – 3896, 2003.
[9] Introduction to PET Physics, University of Washington, https://depts.washington.edu/imreslab/, accessed(2022).
[10] B.J. Wilson, The Radiochemical Manual, The Radiochemical Centre, Amersham, 1966.
[11] M.S. Silberberg, The Molecular Nature of Matter and Change. McGraw Hill, New York, 2013.
[12] Nuclide Chart, https://www.nucleonica.com/wiki/, accessed(2022).
[13] E. Hess, S. Takacs, B. Scholten, F. Tarkanyi, H.H. Coenen, and S. M. Qaim, Excitation function of the ^{18}O(p,n)^{18}F nuclear reaction from threshold up to 30 MeV, *Radiochim Acta*, **89**, 357 – 362, 2001.
[14] J. Pacak, Z. Tocik, and M. Cerny, Synthesis of 2-deoxy-2-fluoro-d-glucose, *Journal of the Chemical Society D: Chemical Communications*, **2**, 77, 1969.
[15] D.D. Ebbing, General Chemistry, 5th Edition, Houghton Mifflin, New York, 1996.
[16] O. Jacobson, D.O. Kiesewetter, and X. Chen. Fluorine-18 radiochemistry, labeling

strategies and synthetic routes, *Bioconjugate Chemistry*, **26**, 1–18, 2015.

[17] Production and Quality Control of ^{18}F-FDG, PETNET Pharmaceuticals Inc, https://pharmacyce.unm.edu/nuclear_program/neolibrary/libraryfiles/fdg_prod_qc.pdf, accessed(2022).

[18] A.R. Sowa et al, Futureproofing [18F]Fludeoxyglucose manufacture at an Academic Medical Center, *EJNMMI Radiopharmacy and Chemistry*, 3, 1 - 12, 2018.

[19] D.L. Bailey, Positron Emission Tomography, Springer, London, 2003.

[20] W. Jiang, Y. Chalich, and M.J. Deen, Review: Sensors for positron emission tomography applications, *Sensors*, **19**, 1 – 57, 2019.

[21] Y.F. Tai and P. Piccin, Applications of positron emission tomography in neurology, *JNeurol Neurosurg Psychiatry*, **75**, 669 - 676, 2004.

[22] A. Buffler et al, PEPT Cape Town: A new positron emission particle tracking facility at iThemba LABS, In Proceedings of International Topical Meeting on Nuclear Research Applications and Utilisation of Accelerators, 1- 8, 2010.

[23] A. Camroodien, M. van Heerden, S. Nair, and T. Leadbeater, Development of ^{18}F Radiochemistry for Positron Emission Particle Tracking (PEPT), The Proceedings of SAIP 2021, 2022.

[24] X. Fan, D.J. Parker, and M.D. Smith, Labelling a single particle for positron emission particle tracking using direct activation and ion-exchange technique, *Nuclear Instruments Methods in Physics Research*, **562**, 345 – 350, 2006.

[25] T. Leadbeater et al, Development of Tracer Particles for Positron Emission Particle Tracking (PEPT), Presented at Accelerator Applications Topical Meeting, Austria, 2021.

[26] D. Parker, C. Broadbent, P. Fowles, M. Hawkesworth, and P. McNeil, Positron emission particle tracking - a technique for studying ow within engineering equipmennt, *Nuclear Instruments Methods in Physics Research*, **326**, 592 – 607, 1992.

[27] D.J. Parker and X. Fan, Positron emission particle tracking - Application and labelling techniques, *Particuology*, **6**, 16 - 23, 2008.

[28] C.R.K. Windows-Yule, Recent advances in positron emission particle tracking: a comparative review, *Reports on progress in physics*, **85**, 1 - 48, 2022.

[29] M.R. Hawkesworth, Non-medical applications of a positron camera, *Nuclear Instrumentation and Methods*, **A310**, 423 – 434, 1991.

[30] D.J. Parker, R. Forster, P. Fowles, and P. Takhar, Positron emission particle tracking using the new Birmingham positron camera, *Nuclear Instruments Methods in Physics Research*, **477**, 540 – 545, 2002.

[31] PEPT Cape Town, http://www.peptcapetown.uct.ac.za/, accessed(2022).

[32] T.J. Spinks et al, Physical characteristics of the ecat exact3d positron tomograph, *Physics in Medicine Biology*, **45**, 2601, 2000.

[33] PHY3004W Group Project, Grappling with Granular Gallimaufries, Department of Physics, University of Cape Town, 2019.

[34] NRF-iThemba LABS Nuclear Medicine Department, https://tlabs.ac.za/nuclear-medicine, accessed(2023).

[35] M. van Heerden, Improving the selectivity of the radiolabelling of ion exchange resin tracers for positron emission particle tracking, Master's thesis, University of Cape Town, 2015.

[36] K.E. Cole, A. Buffler, N.P. van der Meulen, J.J. Cilliers, J-P. Franzidis, I. Govender, C. Liu, and M.R. van Heerden, Positron emission particle tracking measurements with 50 microns tracers, *Chemical Engineering Science*, **75**, 235 – 242, 2012.

[37] T. Leadbeater, Development of direct activation tracer particles for positron emission particle tracking (PEPT), Proposal for beam time, 2017.

[38] J. Reich, Development of direct activation tracer particles using a $^{16}O(\alpha,pn)^{18}F$ reaction for use in positron emission particle tracking (PEPT), Honours thesis, University of Cape Town, 2019.

[39] T. Leadbeater, M. van Heerden, A. Buffler, A. Camroodien, and G. Steyn, proceedings of 30th Conference of the International Nuclear Target Development Society (INTDS), 2022.

[40] G. Steyn et al, 30th World Conf. of the INTDS (International Nuclear Targets Development Society), Germany, 2020.

[41] Bio-Rad SAER Manual: AG1, AG MP-1 and AG2 Strong anion exchange resin instruction manual, https://www.bio-rad.com/webroot/web/pdf/lsr/literature/LIT212.pdf, accessed(2020).

[42] Rohm and Haas, Ion Exchange, https://www.lenntech.com/Data-sheets/, accessed(2021).

[43] Purolite Product Manual, https://www.purolite.com, accessed(2020).

[44] K. Cole, A. Buffler, J.J. Cilliers, I. Govender, J.Y.Y. Heng, C. Liu, D.J. Parker, U.V. Shah, M. van Heerden, and X. Fan, A surface coating method to modify tracers for positron emission particle tracking (PEPT) measurements of froth flotation, *Powder Technology*, **263**, 26 – 30, 2014.

[45] X. Fan, D.J. Parker, and M.D. Smith, Enhancing ^{18}F uptake in a single particle for positron emission particle tracking (PEPT) through modification of solid surface chemistry, *Nuclear Instruments and Methods in Physics Research A*, **558**, 542 - 546, 2006.

[46] D.J. Parker and X. Fan, Positron emission particle tracking (PEPT) — Application and labelling techniques, *Particuology*, **6**, 16 - 23, 2008.

[47] X. Fan, D.J. Parker, and M.D. Smith, Adsorption kinetics of fluoride on low cost materials, *Water Research*, **37**, 4929 - 4937, 2003.

[48] M. Dawood, X. Jiang and K. Schafers, Correction techniques in emission tomography,

CRC Press, Florida, 2012.
[49] T. Leadbeater et al, Development of tracer particles for positron emission particle tracking (PEPT), Nuclear Science and Engineering, **197**, Issue 3, 2023.
[50] BYJU'S Column Chromatography, https://byjus.com/chemistry/column-chromatography/, accessed(2023).

Appendix

* Note all ^{18}F-FDG supplied throughout all trials had a volume of 500 μL.

Table A1 Activity concentration details of the ^{18}F-FDG supplied and the reactive solution, comprising of ^{18}F-FDG, used for radiolabelling with the volume specified in corresponding trials.

trial	AC of ^{18}F-FDG (mCi/μL)	AC of ^{18}F-TFA (μCi/μL)	volume of ^{18}F-TFA (μL)
A1.1	0.068	0.072	150
A1.2		0.068	165
A2.1	0.038	0.036	165
A2.2		0.035	165
A3.1	0.077	0.043	160
A3.2		0.043	160

Table A2 Activity concentration details of the ^{18}F-FDG supplied prior to separation of ^{18}F and glucose-complex and the resultant separated solution, comprising of ^{18}F-TFA complex, used as the reactive solution for radiolabelling with the volume specified in corresponding trials.

trial	AC of ^{18}F-FDG (mCi/μL)	AC of ^{18}F-TFA (μCi/μL)	volume of ^{18}F-TFA (μL)
B1.1	0.042	0.016	280
B1.2		0.016	280
B2.1	0.054	0.023	270
B2.2		0.018	270
B3.1	0.054	0.018	270
B3.2		0.018	270
C1.1	0.020	0.009	350
C1.2		0.009	350
C2.1	0.035	0.022	225
C2.2		0.021	225
C3.1	0.036	0.018	280
C3.2		0.016	280
D1.1	0.029	0.011	290
D1.2		0.011	290
D2.1	0.050	0.029	220
D2.2		0.030	220
D3.1	0.035	0.019	270
D3.2		0.019	270
E1.1	0.029	0.025	280
E1.2		0.024	275
E2.1	0.029	0.010	460
E2.2		0.011	460

trial	AC of ^{18}F-FDG (mCi/μL)	AC of ^{18}F-TFA (μCi/μL)	volume of ^{18}F-TFA (μL)
E3.1	0.059	0.025	270
E3.2		0.025	270
F1.1	0.035	0.007	510
F1.2		0.007	510
F2.1	0.044	0.019	250
F2.2		0.019	250
F3.1	0.050	0.024	250
F3.2		0.022	250

Table A4 Activity concentration details of the ^{18}F-FDG supplied prior to separation of ^{18}F and glucose-complex and the resultant separated solution, comprising of ^{18}F-TFA complex, used as the reactive solution with the volume specified for radiolabelling in corresponding trials. The trials listed below involved pre-treatment of the reactive solution prior to radiolabelling.

trial	AC of ^{18}F-FDG (mCi/μL)	AC of ^{18}F-TFA (μCi/μL)	volume of ^{18}F-TFA (μL)
G1.1	0.038	0.016	450
G1.2		0.015	450
G2.1	0.032	0.012	500
G2.2		0.013	500
G3.1	0.049	0.023	450
G3.2		0.023	450
H1.1	0.041	0.016	480
H1.2		0.017	480
H2.1	0.044	0.018	400
H2.2		0.016	400
H3.1	0.031	0.014	385
H3.2		0.014	385
I1.1	0.041	0.016	470
I1.2		0.016	470
I2.1	0.026	0.011	500
I2.2		0.010	500
I3.1	0.033	0.012	370
I3.2		0.016	370